Osteogenic effect of porous hydroxyapatite scaffolds covered with 45S5 bioactive glass and poly(lactic-co-glycolic acid) composite microfiber

Jeong-Hyun Ryu

Department of Applied Life Science

The Graduate School, Yonsei University

Osteogenic effect of porous hydroxyapatite scaffolds covered with 45S5 bioactive glass and poly(lactic-co-glycolic acid) composite microfiber

Directed by Professor Jae-Sung Kwon

The Doctoral Dissertation
submitted to the Department of Applied Life Science,
the Graduate School of Yonsei University
in partial fulfillment of the requirements for the degree of
Ph.D. in Applied Life Science

Jeong-Hyun Ryu

December 2021

This certifies that the Doctoral Dissertation
of 'Jeong-Hyun Ryu' is approved.

Thesis Supervisor: Jae-Sung Kwon

Thesis Committee Member#1: Kwang-Mahn Kim

Thesis Committee Member#2: Kyung Mi Woo

Thesis Committee Member#3: Jae-Kook Cha

Thesis Committee Member#4: Min-Ho Hong

The Graduate School
Yonsei University
December 2021

ACKNOWLEDGEMENT

"Your beginnings will seem humble, so prosperous will your future be."
[Job 8:7]

I am deeply grateful to everyone who gave supported, encouraged, motivated, and enabled me over the course of my Ph.D. program.

To start, I would like to express the deepest appreciation to my supervisor, *Prof. Jae-Sung Kwon*, who has provided advice and guidance throughout the research, and also encouraged me at every step of the program. I would like to thank to *Prof. Kwang-Mahn Kim*, whose encouragements influenced my research. His words brought me back to ponder upon what 'science' is, and to be true to the basics of science throughout my research. In addition, I would like to thank *Prof. Kyung Mi Woo*, who has given me an opportunity to focus on the Ph.D. course and led me through the field of tissue regeneration during my research. Furthermore, I would like to express my gratitude to *Prof. Jae-Kook Cha*, who made time during his busy schedule to provide valuable clinical situation-related advices for my research, and to *Prof. Min-Ho Hong*, who expanded my knowledge in tissue engineering through his meticulous guidance and detailed feedbacks. Moreover, a debt of gratitude is owed to *Prof. Jung-Hwan Lee*, who first 'pushed' me towards the opportunity to start the doctorate program, and to further develop as a scientist as time passed on.

Last, but not least, I want to extend a huge thanks to all of my colleagues and friends; their everlasting support made it possible for me to focus on my research and encouraged me to keep a steadfast willpower throughout the years. Finally, I can't thank my beloved family enough. I want to thank my parents, *Ji-Yeon Ryu* and *Sun-Jin Cho*, who provided me with their unconditional love and confidence along with never-ending

encouragements from the bottom of my heart. I also want to thank my younger brother, *Seok-Hyun Ryu*, for his big support.

Thanks to everyone once again. This would not have been possible without support from everyone. This is dedicated to you all.

Jeong-Hyun Ryu

TABLE OF CONTENTS

LIST OF FIGURES

LIST OF TABLES

ABSTRACT

Osteogenic effect of porous hydroxyapatite scaffolds covered with 45S5 bioactive glass and poly(lactic-co-glycolic acid) composite microfiber

Jeong-Hyun Ryu

Department of Applied Life Science

The Graduate School, Yonsei University

(Directed by Professor Jae Sung-Kwon, M.D., Ph.D.)

A wide range of synthetic bone graft materials are being used as scaffolds in medical fields such as oral, craniomaxillofacial, and orthopaedic surgery. One of these materials is porous hydroxyapatite (HAp) scaffold, which possess both biocompatibility and osteoconduction properties. However, it is limited in terms of bioactivity and osteoinduction. On the other hands, 45S5 bioactive glass (45S5 BG) well known to high bioactivity, osteoconduction, and osteoinduction. Also, poly(lactic-co-glycolic acid) (PLGA) is an biodegradable polymer

that is well known for its properties including control the rate of degradation. These advantageous properties motivated our study, which aimed to improve the bioactivity and osteoinduction of HAp scaffold covered with PLGA/45S5 BG composite microfiber (HPB scaffold) and to investigate the characteristics of HPB scaffold as bone graft materials.

For experimental purpose, HPB scaffold was prepared by fabricating sponge replica method and electrospinning method. The spinning time differed that it depends on the experimental group, including 10, 20, and 30 minutes. The characteristics of the HPB scaffold were analyzed using scanning electron microscopy-energy dispersive X-ray spectrometry (SEM-EDS), micro computed tomography (μ-CT), and thermogravimetric analysis (TGA). In addition, ion release was detected for 28 days by inductively coupled plasma mass spectrometry (ICP-OES). Fibroblast and preosteoblast were cultured and assessed for cytotoxicity, proliferation and viability. To confirm osteogenic differentiation, alkaline phosphatase (ALP) activity, western blot, immunocytochemistry (ICC), and alizarin red s (ARS) staining were carried out. The results of each test were statistically analyzed with one-way analysis of variance (ANOVA) followed by Tukey's post hoc statistical test ($p < 0.05$).

All HPB scaffolds had a cancellous bone-like structure and they were covered with a layer of composite microfibers containing 45S5 BG atoms (Si-Ca-Na-P) by SEM-EDS. TGA analysis of all HPB scaffolds was confirmed to contain the 45S5 BG in PLGA microfiber. Additionally, these scaffolds enabled to sustain release of Si, Ca, Na, and P ions for 28 days. Cytotoxicity of all HPB scaffold was no significantly difference.

Cell proliferation of HPB scaffolds was increased from 1 day to 3 days ($p < 0.05$). In addition, cell viability on the HPB scaffolds was confirmed with LIVE/DEAD assay. ALP activity and western blot analysis indicated that HPB scaffolds with 20 and 30 minutes of coating induced higher levels of osteogenesis-related markers compared to other scaffolds ($p < 0.05$). Furthermore, ICC indicated osteopontin expression in HPB scaffolds. ARS indicated that HPB scaffolds with 30 minutes of coating were more effective than the other scaffold in terms of mineralization ($p < 0.05$). These results showed that HPB scaffold was successfully fabricated by two step process and 45S5 BG ions were released for 28 days. In addition, HPB scaffold supported both pre-osteoblast proliferation and osteoblast differentiation into bone gene expression to osteoblast phenotype. Therefore, HPB scaffold may be a potential bone substitute for osteogenic activity.

Key words; Hydroxyapatite scaffold, 45S5 Bioactive glass, Poly(lactic-co-glycolic) acid, Osteogenic activity, Bioactivity

Osteogenic effect of porous hydroxyapatite scaffold covered with 45S5 bioactive glass and poly(lactic-co-glycolic acid) composite microfiber

Jeong-Hyun Ryu

Department of Applied Life Science
The Graduate School, Yonsei University

(Directed by Professor Jae-Sung Kwon, M.D, Ph.D.)

I. INTRODUCTION

1. Tissue engineering and regenerative medicine

Tissue engineering is an interdisciplinary field, defined by Langer and Vacanti in early 90s, that applies the principles of engineering and life science to develop biological substitutes that restore, maintain, or improve tissue function (Langer and Vacanti 1993). On the contrary, regenerative medicine, which has a similar meaning to that of tissue engineering, is an interdisciplinary field of research and clinical application focused on the repair, replacement or regeneration of cells, tissues or organs to restore impaired function resulting from any cause, including congenital defects, disease, trauma, and aging (Daar and Greenwood 2007). While

tissue engineering and regenerative medicine may seem interchangeable by definition, the specific term ‘Tissue Engineering’ will be used to describe the field of our research in our study, as the term ‘Regenerative Medicine’ is broader term that covers a wider range of medical field.

We can inform that cells and materials are most important two elements composed of tissue engineering. The researcher who employed in this field has been studied about cells and materials in biomedical field to regenerate to damaged tissues before introduction of conception of tissue engineering. Figure 1 shows the representative of tissue engineering and how they are complementary to each other.

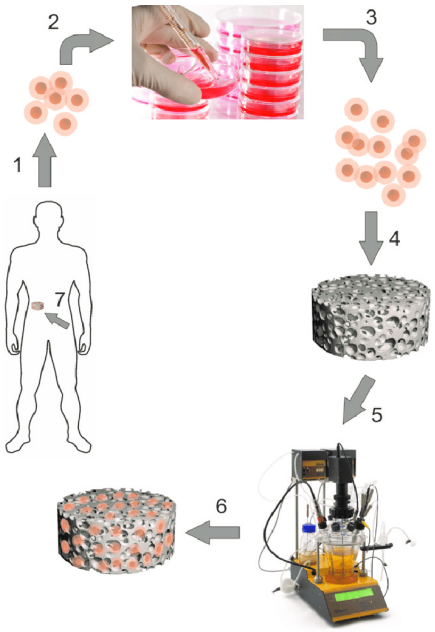

Figure 1. The conception of tissue engineering paradigm. 1: Number of cells are isolated from human body 2: The isolated cells are incubated and subcultured on the culture conditions. 3: The cultured cells are inoculated. 4: The scaffold is seeded to the cultured cell. 5: The scaffold seeded on cultured cells utilizes a bioreactor with growth factor to improve proliferation and differentiation. 6: The scaffold populated in the cells are placed in the culture to further cell number. 7: Finally, the regenerated tissue is implanted into the defect site on the human body (Santos Jr and de Carvalho Zavaglia 2016).

2. Bone regeneration

2.1. Bone structure

Bone is a living, dynamic, and mineralized connective tissue of the human body, and the unique characteristics of bone have the ability to remodel and regenerate itself. The component of bone consists of the inorganic mineral phase (e.g. calcium phosphate, carbonate, sodium and magnesium) and organic phase (e.g. collagen fibers, lipid, peptides, protein and glycoproteins).

On a macroscopic scale, bone is composed of outer dense part; cortical bone (named compact bone) and porous part; inner cancellous bone (named spongy bone or trabecular). The cortical bone is a high density that include less than 10% connective tissue. Cortical bone represents 80% of the skeletal mass and has supports most of mechanical function such as stiffness, strength and toughness. Cortical bone has a much denser structure with a porosity of 3 – 12 % and an average density of 1.80 g/cm^3. On the other hands, cancellous bone is 20% of the skeletal mass and consists of connective tissue. It is located within metaphysis, epiphysis, and medullary cavity at the end of long bones, and in short bone as well. Cancellous bone has a porosity of 50 – 90% with an average cancellous spacing of around 1 mm and an average density of 0.2 g/cm^3. However, its metabolic activity such as bone cell production and mineral exchange is higher in cancellous bone compared to cortical bone (Bilgiç et al. 2020; Henkel et al. 2013; Monier-Faugere, Langub, and Malluche 1998).

On a microscopic scale, osteon (or havarsian system) is cylindrical structure that contains a mineral matrix. The central canal of an osteon contains cells, vessels and nerves and the canals connecting osteons are called haversian canals. Lamellae in osteon are composed of mineralized collagen fibres and stacked parallel to form layer.

On a nanostructure level, the most prominent structure are the collagen fibres,

surrounded and infiltrated by mineral. At the sub-nanostructure level, there can be divided into bone crystals, collagen molecules, and non-collagenous organic proteins (Henkel et al. 2013; Lacroix 2019).

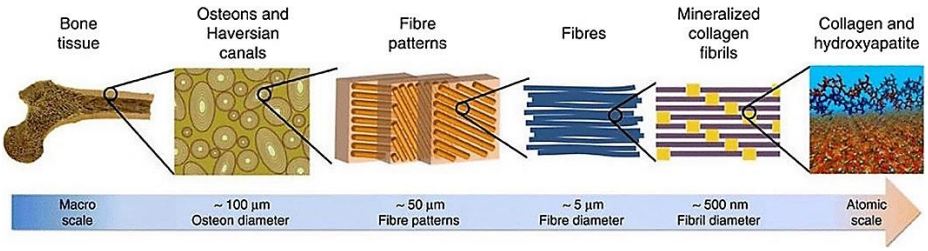

Figure 2. Hierarchical structural organization of bone ranging from macroscale skeleton to nanoscale collagen and HAp (Nair et al. 2013).

Bone also can be separated into three main components: bone matrix, bone cells, bone marrow and its associated vascular network. Bone matrix has activity of mineral storage, mechanical support and exerts essential role in the bone homeostasis. Bone cells work in harmony to maintain balance between bone formation and bone resorption, ultimately to control bone structure and function. The bone marrow supplies the many of stem cell (e.g. hematopoietic stem cells, and multipotent stromal stem cells), blood product, and interaction with the tissue and organs.

2.1.1 Extracellular bone matrix

All tissues and organs contain a mixture of cells and non-cellular components, which form well-organized networks called extracellular matrix (ECM). The ECM provides the tissue that both biochemical and essential structural support for its cellular constituents. In terms of bone, bone ECM is composed of organic collagen fibers and inorganic bone mineral crystals. Organic fibers consisted of collagen which are the most abundant in bone ECM. The main function of collagens is mechanical support such as tensile strength and regulate cell adhesion, support chemotaxis and migration (Kusindarta and Wihadmadyatami 2018; Sartori et al. 2015). There are various type of collagen, 28 different types have been identified, described, and divided into several group according to the structure they form. Above all, type I collagen (COL-I) is representative in organic collagen fibers of bone ECM, which is 90% of the total collagen in bone tissue and forms (Varma, Orgel, and Schieber 2016).

In terms of the bone mineral, the main component of inorganic phase is usually referred to hydroxyapatite (HAp; $Ca_{10}(PO_4)_6(OH)_2$). The apatite in bone is structurally disordered, and compositionally nonstoichiometric due to the presence of a substantial amount of anionic (e.g. HPO_4^{2-}, CO_3^{2-}) and cationic (e.g. Na^+, Mg^{2+}) species, together with the presence of ion vacancies into the crystal lattice (Von Euw et al. 2019). For instance, bone mineral is initially deposited as an amorphous calcium phosphate (ACP), along with large amounts of calcium carbonate. The carbonate content plays a role in mineral crystals growth, becoming more plate-like, and orient themselves parallel to one another and to the collagen fibrils. ACP are known as their Ca/P ratio varying between 1.2 and 2.2. The deposition of ACPs produces as source of HAp crystallite nucleation and growth (Jiang et al. 2017). Other organics also promote the initial nucleation and biological apatite deposition, apatite size, and growth rate of the crystals (Boonrungsiman et al. 2012).

The non-collagenous proteins of bone matrix are composed of proteoglycans and glycosaminoglycans. There are four major protein; bone sialoprotein (BSP), osteopontin (OPN), osteocalcin (OCN), and osteonectin (ON). These are related to growth the bone cells and regulated bone mineralization and remodeling.

BSP is an acidic, phosphorylated glycoprotein that is synthesized by osteoblasts and osteoclastic-like cells in culture. BSP is involved in regulating HAp crystal formation in bones. It exhibits a limited pattern of expression and its expression is associated to mineralization. BSP expression marks a late stage of osteoblastic differentiation and an early stage of matrix mineralization. On the other hands, OPN is an acidic, phosphorylated glycoprotein as BSP in same family known as SIBLING (small integrin-binding ligand, N-linked glycoprotein). OPN is consider to play important role mineralization in bone, which inhibit the mineral formation and crystal growth (Denhardt and Guo 1993). OPN also binds to osteoclasts and promotes the adherence of the osteoclast to the mineral in bone during the resorption process (Si et al. 2020).

OCN is the most abundant non-collagenous protein in bone matrix, and it enhanced calcium binding and controls mineral deposition. OCN is a 49-residue protein that exists as a tertiary structure after carboxylation, with the resulting residues expected to provide a strong binding affinity for the HAp (Tavakol and Vaughan 2020). The recent researches have demonstrated that OCN is activated and regulated to bone formation by osteoblasts and osteocytes in bone remodeling process (Huang et al. 2007; Xiong and O'Brien 2012).

ON is a non-collagenous protein in bone matrix expressed in mineral tissues and is expressed in osteoblast. ON is known for the affinity to HAp and collagen and is involved in bone development. It may promote nucleation of new mineral crystals and play a role in osteoblast proliferation (Hunter et al. 1996).

2.1.2 Bone cells

There are many cells associated with bone, and they are divided into three major types of cell; osteoblasts, osteocytes, and osteoclasts (Figure 3).

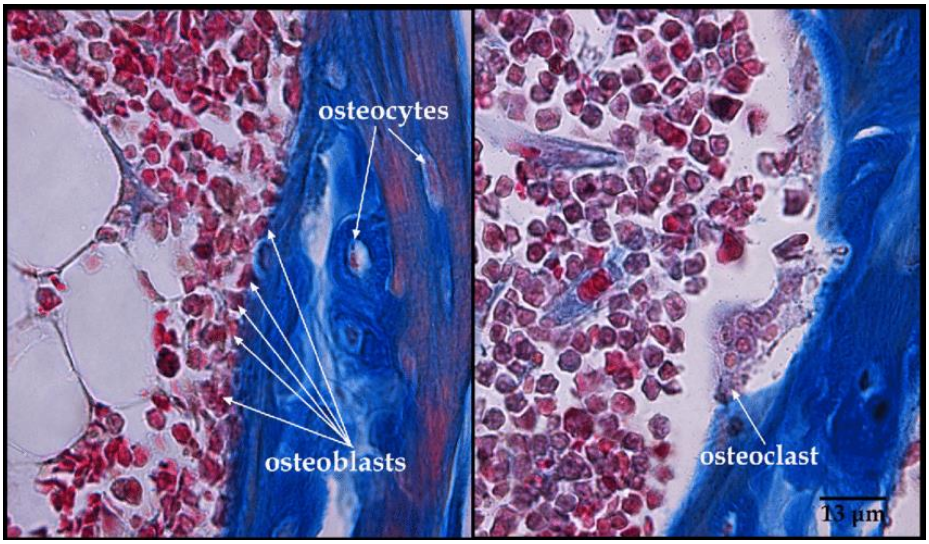

Figure 3. Histological image of bone cells of indicated to osteoblasts, osteocytes, and osteoclasts (Filipović and Šošić-Jurjević 2012).

Osteoblasts are cells of mesenchymal origin that secrete extracellular matrix proteins and promote mineralization for the bone structuring and remodeling process. Osteoblast have a well-developed golgi apparatus and euchromatic nucleus. Osteoblasts carried out the function of bone matrix protein secretion and bone mineralization. Osteoblasts are high level expression of alkaline phosphatase (ALP) and OCN that effect the bone formation (Bilgiç et al. 2020). Osteoblasts secrete COL-I which is assembled into collagen fibrils and serves as a template for the following bone mineral deposition in the form of HAp

(Shapiro 2016).

Osteocytes are former osteoblasts that become entombed during the process of bone deposition and regularly distributed throughout the bone mineralization. Osteocytes are the longest living bone cell, making up 90 – 95 cells in bone tissue in contrast to osteoclasts and osteoblasts making up ~5% (Bonewald 2007). Osteoblasts are individually encased in lacunae and exhibit cytoplasmic dendritic process that run along narrow canaliculi within the mineralized bone matrix. Respectively, osteocytes can make and resorb the bone by different mechanism. Osteocytes are the regulator of bone through their direct regulation of calcium abundance in mineralization and indirect control of osteoblasts and osteoclast activities (Florencio-Silva et al. 2015).

Osteoclasts are the primary and giant multinucleate cells which involved in resorption of bone mineralization in bone remodeling of extracellular matrix. For bone remodeling to occur in physiological conditions, osteoclast precursors from monocytes or macrophages recruited to bone surface and activate the proliferation by differentiation to osteoclasts (Xu and Teitelbaum 2013). Active osteoclasts has the formation that enable osteoclasts to attach to the bone surface, acidify and degrade the mineralized matrix, and migrate along the bone surface. After activity of osteoclast for bone resorption, osteoclasts occur the apoptosis (Arnett and Orriss 2018).

2.1.3 Bone formation and fracture healing

Bone is a highly specialized supporting framework of the body. It is characterized by its rigidity and hardness and is endowed with the power of regeneration and repair (Kini and Nandeesh 2012). During the development of bone, it occurs through two distinguishing process; intramembranous ossification and endochondral ossification. Intramembranous ossification is group of mesenchymal stem cell within a highly vascularized area of the embryonic connective tissue that proliferates and differentiates directly preosteoblasts and then into osteoblasts. Endochondral ossification occurs that mesenchymal stem cells transform a chondroblasts and a hyaline cartilage template is formed over time replaced by mineralized bone tissue (Stoddart et al. 2018). Finally, it is practically recognizable the mature bone formed by both processes. However, the mechanism of both process which route is taken are difficult to understand.

The bone fracture is one of the more common injuries among the bone disease. The aim of bone fracture healing process is prompt stabilization of broken parts at damaged bone. According to this mechanism in bone fracture healing process, cell death (necrosis) and hematoma occurs with bone fracture and inflammatory cells response the area for cleaning before restoration. Following the inflammation, revascularization which is the process by new blood vessels occurs the supplementary of oxygen. Then, the repair phase follows initial stabilization by deposition of collagen and cartilage (soft callus) is replace with a bone (hard callus) connecting bone fragments with new bone. Finally, the bone remodeling phase occurs by coordinated osteoblast and osteoclast activity over a span of several months (Ghiasi et al. 2017; Wang and Yeung 2017).

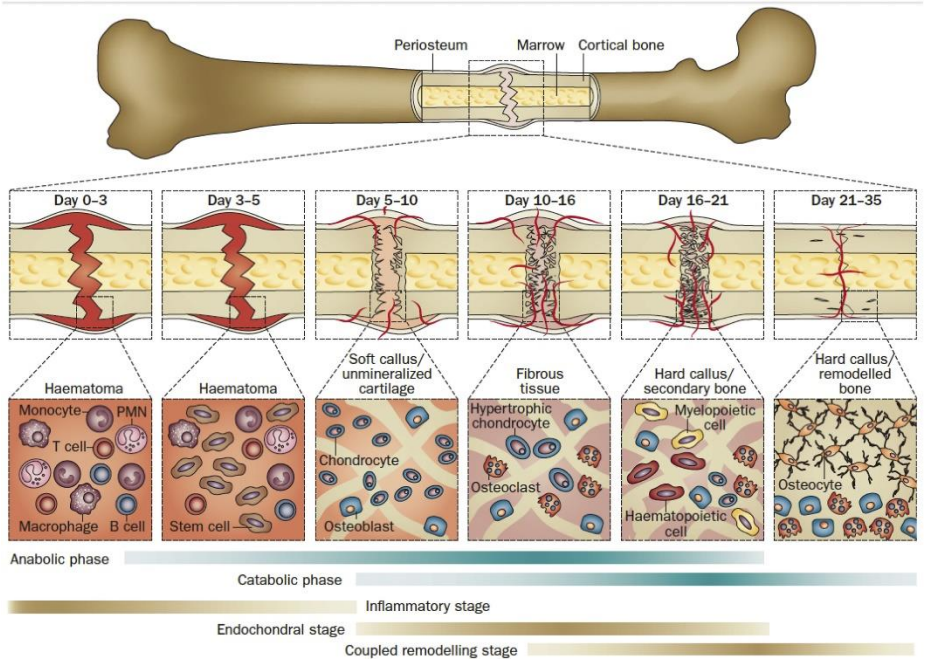

Figure 4. Bone fracture healing process (Einhorn and Gerstenfeld 2015).

2.2. Bone grafting

Bone grafting is a surgical procedure that transplanted bone to repair and reconstruction for diseased or damaged bone. More than 2.2 million bone graft procedures are annually performed around the world for repairing the bone defects in oral, craniomaxillofacial, and orthopaedics (Campos et al. 2018). Bone graft has different characterization such as source, origin (e.g. natural or synthetic), composition, porosity, crystallinity, processing of the materials, biological performance. The ideal bone graft is important that understanding requirement of the specific properties consider the patients in clinical environments (Baldwin et al. 2019; Fernández et al. 2015).

2.2.1 Biological mechanism of bone graft substitute

The physiological properties of osteoconduction, osteoinduction, and osteogenesis process by bone graft is three important factors in bone regeneration. They can be characterization as follows (Albrektsson and Johansson 2001; Khan et al. 2005; Moore, Graves, and Bain 2001; Roberts and Rosenbaum 2012; Wang and Yeung 2017):

Osteoconduction is the process by which an implanted bone grafting material from host bone passively allows ingrowth of capillaries, perivascular tissue, and mesenchymal stem cells from the host site along the implanted bone grafting materials.

Osteoinduction is the ability to induce recruitment, proliferation and differentiation of the mesenchymal stem cell from the around tissue to an osteoblastic phenotype.

Osteogenesis occurs the formation of new bone by osteoblastic cells from mesenchymal stem cell within graft materials. Therefore, osteogenic bone graft has all the cellular elements, growth factors and scaffolding required to form new bone formation.

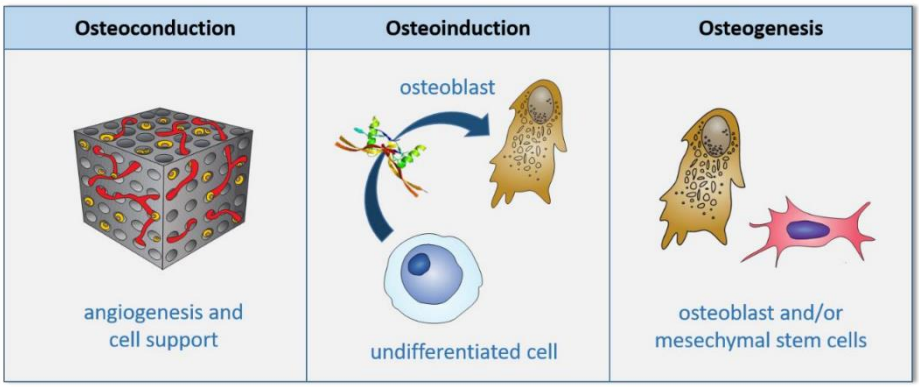

Figure 5. Schematic of osteoconduction, osteoinduction, and osteogenesis (Özcan et al. 2021).

2.2.2 Classification of bone graft

Bone grafting is normally used as a surgical procedure that replace the trauma or damaged bone in order to regenerate bone, and the bone graft is important that substitute materials play a role in reconstruction oral, craniomaxillofacial, and orthopaedic surgery (Kumar, Vinitha, and Fathima 2013; Nandi et al. 2010). The bone graft materials classified the autografts, allografts, xenografts, and alloplasts.

Autografts are commonly obtained from a patient's own tissue. Autografts provide osteoconductive, osteoinductive, and osteogenesis properties. In addition to advantage of autografts, autografts that is histocompatibility, immunogenicity and highest biological safety have been gold standard. However, supply of autograft is limitation in the case of patients with a damaged or trauma bone, and associated with higher surgical costs and risks (Schmidt 2021).

Allografts are supplementary or substitute in order to solve the limitation of autografts. Allografts harvested from the donor bone tissue of cadaver are prepared in fresh-frozen cancellous bone and marrow, as the freeze-dried bone or demineralized freeze-dried bone (de Alencar and Vieira 2010). The properties of allografts are osteoconduction and osteoinduction but no osteogenesis due to deficiency osteogenic cell. The advantages of allografts are no morbidity of donor site, unlimited use of materials, and availability in mechanical support with various shape and sizes. Despite of advantages of allografts, allografts have several problems. Allografts has potential infection risks by virus (e.g. HIV (human immunodeficiency virus) or hepatitis C) bacterial infection, and immune rejection (Khan et al. 2005; Lomas, Chandrasekar, and Board 2013; Mroz et al. 2008).

Xenografts derived from different species (e.g. bovine, porcine, or ovine) are the substitute materials. Xenograft need viral inactivation in that all proteins as well as the cells must be eliminated due to immunogenicity of different species (Murugan, Rao, and Kumar 2003). The advantages of these materials are biocompatibility, natural structure similar to human bone and osteoconduction. However, xenografts have problems to the deficiency of osteoinduction and osteogenesis.

Alloplastic grafts (or synthetic bone grafts) have been developed over past decades and are presently used for clinician in the market. The greatest advantage of these materials is that they do not exposure the disease risk and transfer the virus and possible to shape, porosity, and chemical composition (Hing 2005). Synthetic bone grafts can be suitable to biocompatibility, and most are osteoconduction. Synthetic bone grafts were various in terms of these materials properties such as the characterization, biodegradation rate, and cell response (Bohner 2010; Denry and Kuhn 2016). Representatively, Synthetic bone grafts can be categorized about two parts: polymer-and ceramics-based synthetic bone graft.

The polymer-based bone graft can be categorized into natural and synthetic polymers. The type of biodegradable and non-biodegradable polymer was divided into natural and synthetic polymers. Number of bone graft on the market were commonly used to ceramics-based bone graft included that CaP materials and bioactive glass. These materials consider to varying in terms of materials properties, physical characterization, and biological response (Hing 2005; Mondal et al. 2018; Xu et al. 2017).

2.2.3 Polymer-based bone graft

Polymer-based bone graft can be divided further as non-degradable and degradable. The type of non-degradable polymer is poly (methyl methacrylate) (PMMA) and poly (ether-ether-ketone) (PEEK). PMMA is well-known to biocompatible, biologically inert, and have good mechanical properties. Due to good mechanical properties and stability of PMMA, PMMA is durable to use as bone cement or substitute materials for suitable implants (Arora et al. 2013). Likewise, PEEK has biocompatibility with no cytotoxic effect and good mechanical properties. In these characterizations of PEEK, PEEK is continuously to use as implant materials with clinical applications such as dental and orthopaedic field (Najeeb et al. 2016). On the other hands, degradable polymer bone graft has been commonly investigated for bone regeneration. This substitute has beneficial effect in comparison with non-degradable polymer. The advantages of these substitutes had ability to be absorbed by the body and regenerated without remaining implanted materials. Another advantages of these materials had reaction of hydrolysis in the long-terms implantation upon exposure to body fluids, cellular response, and enzymatic degradation and can be fabricated to a desirable shape to be suitable for the patient in the clinical environment (Nair and Laurencin 2007; Tamariz and Rios-Ramírez 2013). The type of degradable natural polymer is currently available for chitosan, collagen, gelatin and fibrin. On the other hands, the type of degradable synthetic polymer is currently available for poly glycolic acid (PGA), poly lactic acid (PLA), Poly (lactic-co-glycolic acid) (PLGA) and polycaprolactone (PCL) (Vroman and Tighzert 2009).

2.2.4 Ceramic-based bone graft

The bone grafts are commonly being used in dentistry and orthopedics. Bone reconstruction procedures are classically treated by replacement with autografts or allografts. However, supply of autografts or allograft is limitation in the case of patients or donor (Baldwin et al. 2019). Therefore, ceramic-based bone graft are developed as an alternative choice (Moore, Graves, and Bain 2001). Ceramics-based bone graft are component of inorganic properties, which can be fabricated in a variety of structures, porosity, composition, and using a different manufacturing method such as sponge replica method. Ceramics-based bone graft has advantages that have similarity of nature human bone structures and promote the adhesion, proliferation, migration, and osteogenic expression of osteoblastic cells leading to the new bone formation (Baldwin et al. 2019; Panseri et al. 2021; Zimmermann and Moghaddam 2011).

The type of ceramics-based bone graft is CaP material. One of CaP materials is representatively hydroxyapatite (HAp; $Ca_{10}(PO_4)_6(OH)_2$). HAp is one of the most stable and less-soluble calcium phosphate bioceramics with Ca/P ratio of 1.67. HAp is the primary mineral component of bone and attempt to synthetize the HAp and to fabricate a variety type of structure. HAp has excellent biological properties such as biocompatibility, bioactivity, cell migration, and osteoconduction. Despite of these advantages of HAp, its reactivity with existing bone tissue in defected bones is low. In fact, the minimal degradability of HAp in physiological circumstance often results in the materials not being absorbed or replaced by new bone formation (Samavedi, Whittington, and Goldstein 2013; Zhao et al. 2011).

2.3. Poly(lactic-co-glycolic) acid

Above mentioned to polymer-based bone graft (2.2.3), Poly(lactic-co-glycolic) acid (PLGA) is biodegradable polymer in type of the synthetic polymers. PLGA is a linear copolymer that can be prepared at different ratios between its constituent monomers, lactic and glycolic acid. Lactic acid can be isolated from the fermentation of corn or other grains (Gupta and Kumar 2007). Glycolic acid could be obtained by the biochemical enzymatic reaction or by chemical synthesis with chloroacetic acid and sodium hydroxide. The synthetic strategies for PLGA is the ring-opening polymerization of lactide and glycolide (Erbetta et al. 2012).

PLGA has been approved by Food and Drug Administration for human treatment, which is appropriate to bone regeneration for various reason (Danhier et al. 2012). First of all, PLGA has excellent biocompatibility due to eliminating only lactic acid and glycolic acid from the metabolic cycle. Secondly, PLGA has ability to use a variety of process to prepare scaffold, membrane, and micro-/nanoparticle. Thirdly, the biodegradability of PLGA can be flexibly controlled by adjusting the ratio of lactic acid and glycolic acid. The various ratio of lactic acid and glycolic acid have different degradation rate for controlled release. Fourthly, PLGA has appropriate mechanical strength for supporting the defect area in the early stage. Finally, PLGA can be incorporated with a variety of bioceramics such as CaP materials, bioactive glass and a various bioactive factor such as growth factors, drugs, stem cells to promote regeneration of bone defect (Anand et al. 2010; Gentile et al. 2016; Qi et al. 2013; Wang et al. 2018). In previous studies, *in vitro* studies have been reported that PLGA based bone substitutes enhanced osteogenic proliferation and differentiation. Based on the *in vitro* studies, numerous *in vivo* studies have been demonstrated that the various type of PLGA form used as membrane, scaffold, and drug carrier effect on the bone repair in the bone defect of animal model (Lee et al. 2013; Magri et al. 2019; Wang et al. 2017; Zhao et al. 2021).

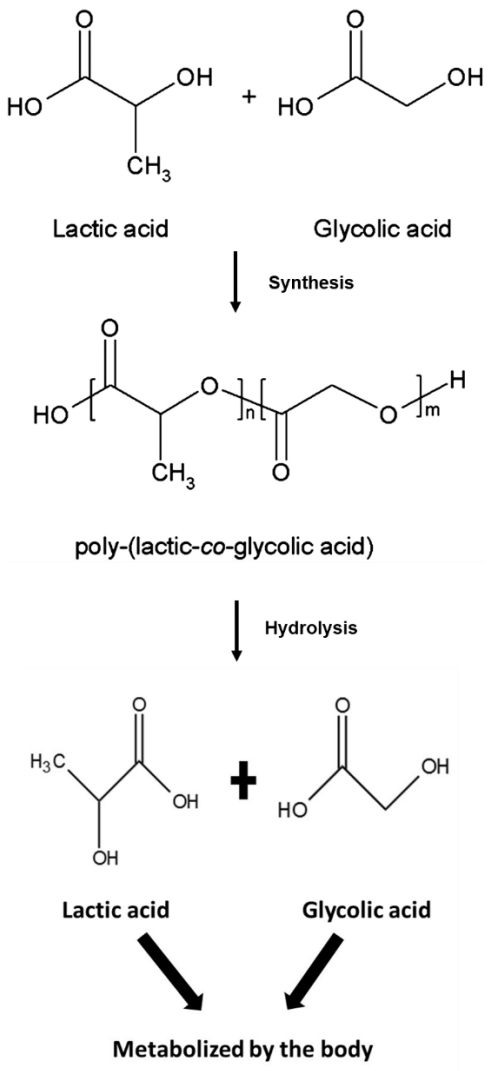

Figure 6. Chemical structure of PLGA and biodegradability of PLGA based on the hydrolysis (Gentile et al. 2014).

2.4. 45S5 Bioactive glass

2.4.1. Current applications

Bioactive glass (BG) is silicate-based glass that has bioactivity. BG has been widely applied as a ceramics-based synthetic bone graft to affect restorative ion to activate the expression of osteogenic and promote the cell proliferation and differentiation (Hench and West 1996; Jones 2013; Ojansivu et al. 2018). Especially, 45S5 bioactive glass (45S5 BG) is the development first bioactive glass that was invented by Larry Hench in 1969. 45S5 BG is glass of the composition 46.1 mol% SiO_2, 26.9 mol% CaO, 24.4 mol% Na_2O, and 2.6 mol% P_2O_5, with resulting from biocompatibility and bioactivity (Hench and West 1996; Hench 2006). It has been beneficially regenerated bone as bone substitutes in the dentistry and orthopedics fields. In clinical trials, it has been reported that 45S5 BG was successfully exploited for bone regeneration in more than 1.5 million patients (Baino, Hamzehlou, and Kargozar 2018; Jones et al. 2016). 45S5 BG has ability to form the hydroxyl carbonate apatite (HCA) layer which is like mineral constituent of bone, it bonds firmly with living bone and tissue. On 45S5 BG subjection in physiological fluids, it formed strong bonds between implant materials and the existent bone tissue from beneficial intracellular and extracellular response (Marelli et al. 2011; Rahaman et al. 2011). It attributed to respond to induce the release and exchange of critical concentration of soluble silicon (Si), calcium (Ca), sodium (Na), and phosphorous (P) ions (Chen, Thompson, and Boccaccini 2006; Hench and West 1996).

2.4.2. Mechanism of mineralization on bioactive glass

After 45S5 BG implanted in human body, it starts reactions at the 45S5 BG surface. The bond between 45S5 BG and bone tissue is formed of HCA layer, which interacts with the collagen fibrils of damaged bone tissue (Jones 2013; Rahaman et al. 2011). In the formation of the HCA layer, dissolution of ionic product coming from 45S5 BG surface was high reactive and accumulating in the environment of physiological pH and variations in the chemical composition of the solution. The mechanism of HCA layer formation interacts between material and physiological fluids responds the first five stages are summarized below (Hench 1991; Huang et al. 2006):

Stage 1. Alkali ions (e.g., Na^+, Ca^{2+}) exchange on the surface and H^+ or H_3O^+ ions coming from the surrounding environment. The reaction occurs very fast, within a few minutes of exposure to physiological fluids.

$$Si\text{-}O\text{-}Na^+ + H + OH^- \rightarrow Si\text{-}OH + Na^+ (aqueous) + OH^-$$

Stage 2. Soluble silica is released from $Si(OH)_4$ to the resulting from break of Si-O-Si bonds and silanol groups (Si-OH) are exposed on the surface of the material.

$$Si\text{-}O\text{-}Si + H_2O \rightarrow Si\text{-}OH + OH\text{-}Si$$

Stage 3. Silanol groups condensation and re-polymerization of an amorphous silica-rich layer on the surface of the glass reduced in Na and Ca

$$Si\text{-}OH + OH\text{-}Si \rightarrow -Si\text{-}O\text{-}Si- + H_2O$$

Stage 4. Migration of Ca^{2+} and $(PO_4)^{3-}$ ions from the glass through the Silica-rich layer. On the silica-rich layer forms, which is component of amorphous calcium phosphate (ACP).

Stage 5. Crystallization of ACP layer incorporates OH^- and $(CO_3)^{2-}$ from the solution and form an HCA layer.

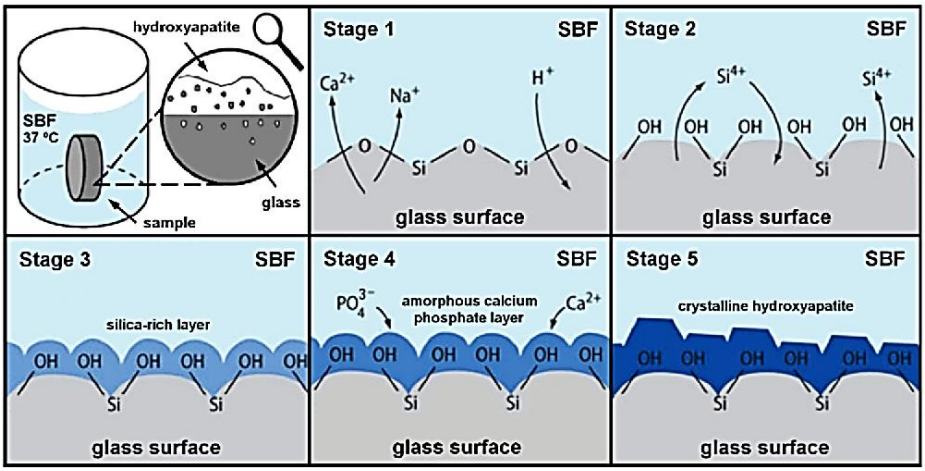

Figure 7. Mechanistic scheme described by an order of reactions of the bioactive glass surface with simulated body fluid (SBF) (Hench 1991).

3. Electrospinning

Electrospinning derived from electrostatic spinning is a method that uses electric force to draw charged threads from polymer solutions. It involves the electrohydrodynamic process, during which a liquid droplet is electrified to generate a jet, followed by stretching and elongation to generate fibers. The major component of electrospinning setup included spinneret section, a high-voltage power supply, and a metal collector. The major component of electrospinning setup included a high voltage power supply, a syringe pump, spinneret (syringe with metallic needle), and conductive collector. The electrospinning process can be divided into following steps. Electrostatic repulsion of the charged polymer solution as using of high voltages is charging of the liquid droplet and conical shape called Taylor cone. The Taylor cone from charging of the liquid droplet extended a straight line. The thinning of the Taylor's cone is elongated by a whipping instability in the presence of an electrical field. As the Taylor cone dries in flight, the mode of current flow changes from ohm to convective as the charge migrate to the surface of the fiber. It is finally deposited on the grounded collector. As it does so, the elongation and thinning of the fibers by the stage of bending instability leads to the formation of homogeneous fibers. For a successful process, the solution, processing, and environmental parameters have to be intended. The solution needed to have viscosity, polymer concentration, molecular weight, conductivity, and surface tension. The processing parameters included the applied voltage, needle to collector distance, and dispensing rate. Environmental parameter consisted of relative humidity and temperature (Dziemidowicz et al. 2021; Li and Xia 2004; Sun et al. 2014).

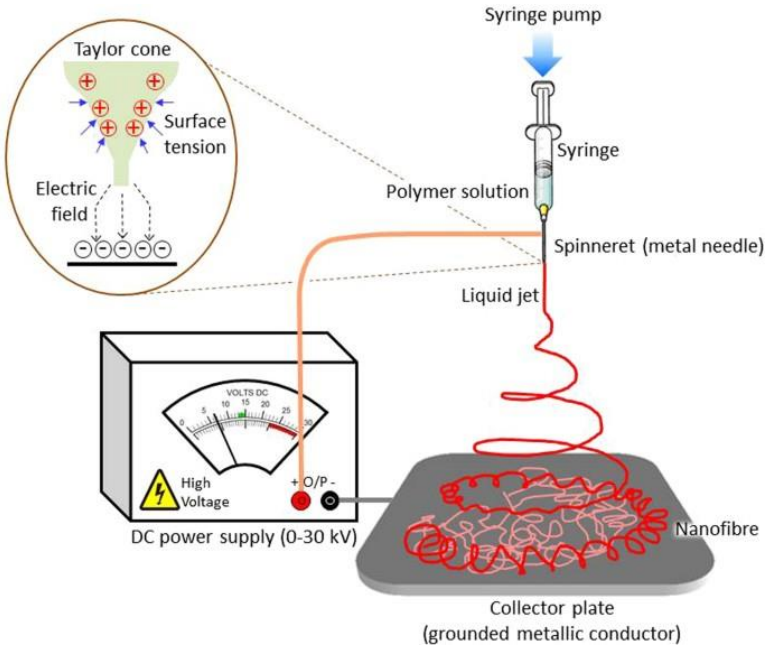

Figure 8. Schematic diagram of electrospinning principle and process (Ghosal et al. 2018).

4. Research objectives

Many studies had investigated the combination of HAp and 45S5 BG for overcoming the disadvantages of HAp. However, the phases of HAp and 45S5 BG changed by high temperature considering that each of HAp and 45S5 BG had different sintering temperature. The combination of 45S5 BG with HAp via sintering were unable to preserve the bioactivity of 45S5 BG (Bellucci et al. 2015; Demirkiran et al. 2011). To overcome the disadvantage of the combination of 45S5 BG with HAp via sintering, fibers consisting of PLGA were applied to preserve the properties of both HAp and 45S5 BG. In view of the above-mentioned PLGA (2.3), PLGA is an FDA-approved biodegradable biopolymer that is well known for including biocompatibility. In particular, PLGA can control the rate of degradation by the ratio of lactide to glycolide. In this advantage of PLGA, the fibrous structure of PLGA obtained using electrospinning has been previously adopted for the controlled release of growth factor, drugs, and bioactive materials (Chen et al. 2015; Hong et al. 2018; Kim et al. 2004). Therefore, 45S5 BG was applied together with biodegradable PLGA to compensate for the disadvantage of HAp. To the best of our knowledge, HAp scaffold is desirable to be covered with electrospun 45S5 BG-incorporated PLGA microfibers, which has the advantage of osteogenic property.

Hence, the aim of this study was to develop a porous HAp scaffold which is covered with PLGA microfiber layer containing 45S5 BG on the sidewall (named HPB scaffold from hereon), and to investigate the proliferation and differentiation of peripheral osteoblasts cultured on the developed scaffold. The null hypotheses were: 1) components of HPB scaffold would not significantly differ from that of HAp scaffold, 2) ion release of HPB scaffold would not significantly differ from that of HAp scaffold, and 3) osteogenic effect of HPB scaffold would not significantly differ from that of HAp scaffold.

II. MATERIALS AND METHODS

1. Fabrication of HAp scaffold

The porous HAp scaffolds were fabricated with the 60 pores per inch (ppi) polyurethane (PU) foam by sponge replica method. As a binder 1 g of poly (vinyl butyral) (PVB)(Sigma Aldrich, St.Louis, MO, USA) were stirred vigorously in 20 mL of absolute ethanol for 2 h and 6 g of HAp powders (Ossgen, Daegu, Korea) were added in the stirring PVB solution. The mixture was stirred for an additional 24 h. 60 ppi PU foam templates were punched to form cylindrical three-dimensional shape (diameter: 10 mm, height: 10 mm) and immersed in the HAp slurry. After blowing with an air gun to disperse the slurry uniformly throughout the porous scaffolds without blocking the pores, the sponges were dried at 90 °C for 30 min. These dipping and drying steps were totally repeated twice. The sponge penetrated HAp slurry was heat-treated to burn out the sponge and binder at 600°C for 1 h in air at a heating rate of 5 °C/min in an electric furnace (Lindberg, Asheville, NC, USA). After burning out the sponge and binder, HAp scaffold was sintered at a 1250 °C for 3 h at heating rate 5 °C/min in an electric furnace. The three-dimensional shape of sintered HAp scaffold was diameter 7 mm and height 9 mm.

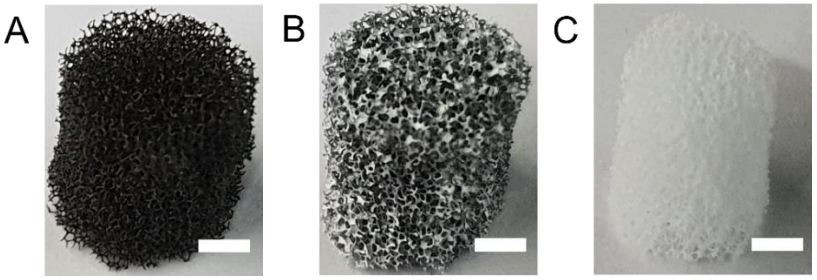

Figure 9. Process of fabrication of HAp scaffold by sponge replica method. (A) 60 ppi PU form, (B) 60 ppi sponge coated by HAp slurry, and (C) Sintered HAp scaffold (Scale bar is 2 mm).

2. Fabrication of HPB scaffold

To prepare electrospinning dope, poly(D,L-lactide-co-glycolide) 6535 (PLGA 6535; M_w 24,000 – 38,000) (Sigma Aldrich, St.Louis, MO, USA) was dissolved in 2,2,2-trifuoroethanol (TFE) (Sigma Aldrich, St.Louis, MO, USA) at a concentration of 0.5 g/mL, and the 45S5 BG (Vitryxx, SCHOTT, Landshut, Germany) was dispersed (45S5 BG:PLGA = 1:10) by vortex agitation and sonication for 10 min. The prepared PLGA solution with 45S5 BG was covered with the sidewall of the HAp scaffolds through the electrospinning (NanoNC, Seoul, Korea) process. The HAp scaffolds were mounted on a metallic stick that would replace the rotating drum of the electrospinning apparatus (Figure 10). In details, the PLGA solution with 45S5 BG was loaded in a syringe pump, and the solution was pumped towards the rotating stick at a rate of 1 mL/h through a 23-gauge metallic needle. The stick with mounted HAp scaffolds was rotated at a speed of 230 rpm with applied voltage of 13 kV. The overall spinning time differed depending on the experimental groups, including 10, 20, and 30 min (Table 1).

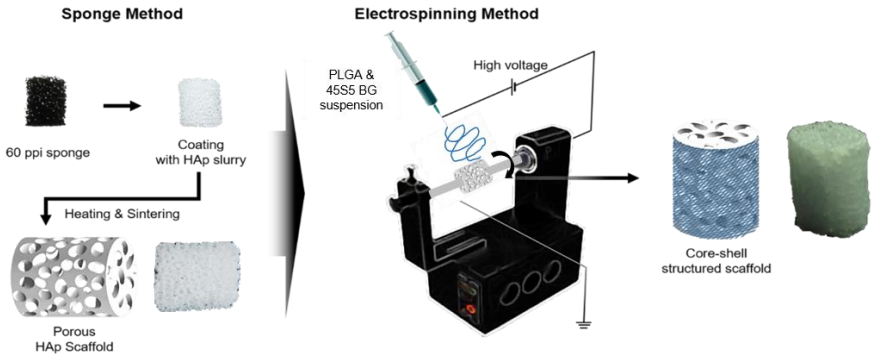

Figure 10. Schematic representation for fabrication of porous HAp scaffold covered with 45S5 BG contained PLGA microfibers layer (HPB scaffold).

Table 1. Control HAp and experimental HPB scaffold used in this study

	HAp group	HPB groups		
		HPB10 group	HPB20 group	HPB30 group
Spinning time of 45S5 BG contained PLGA microfiber	-	10 min	20 min	30 min

3. Characterization of HPB scaffold

3.1. Surface morphology and elements analysis

To observe the morphology and structure of HPB scaffold, the surface morphology of the scaffold was observed by means of scanning electron microscopy (SEM; JEOL, Tokyo, Japan). Briefly, the scaffolds were coated with platinum using a sputter coater with gas pressure of 45 mTorr and 40 mA current for 150 seconds. The coated scaffolds were analyzed at an accelerating voltage of 20 kV. Based on these conditions, the top and bottom of HPB scaffolds were observed. The sidewall of HPB scaffolds was tilted and observed. Energy dispersive spectroscopy (EDS) was used to provide qualitative information on the elemental composition in scaffolds.

Figure 11. Photograph of scanning electron microscopy (SEM; JEOL, Tokyo, Japan).

3.2. Micro-computed tomography analysis

To measure the porosity of HPB scaffold, HPB scaffolds were scanned by micro-computed tomography (micro-CT, SkyScan 1076, Bruker, Billerica, MA, USA). The micro-CT scanner setting operated at 100 kV and 100 μA, and 360° rotation with a pixel size of 36 μm. The 3D images of HPB scaffold were obtained by 3D reconstruction and the porosity of HPB scaffold were calculated from their respective micro-CT images using the Amira graphic program (Mercury Computer System, Berlin)

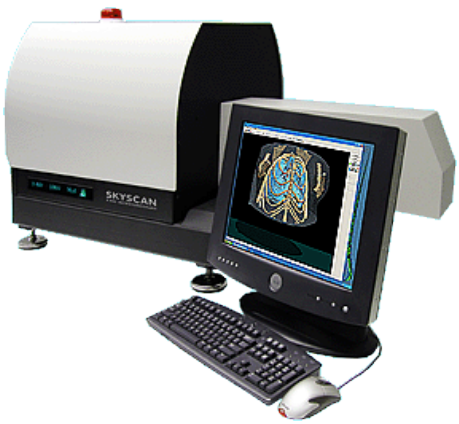

Figure 12. Photograph of micro-computed tomography (μ-CT, SkyScan 1076, Bruker, Billerica, MA, USA).

3.3. Thermogravimetric analysis

To confirm the thermal characterization of HAp, 45S5 BG, and PLGA and compare with residual powders weight with theoretical weight of 45S5 BG particle in the PLGA microfibers separated from HPB scaffold, thermogravimetric analysis (TGA) was conducted on a TGA Q50 analyzer (TA Instrument, New Castle, DE, USA) device from room temperature to 500 °C under nitrogen atmosphere at a heating rate of 10 °C/min.

Figure 13. Photograph of thermogravimetric analysis (TA Instrument, New Castle, DE, USA).

3.4. Ion release analysis

To confirm ionic concentration of released Si, Ca, Na, and P in HPB scaffold, 1 g of HPB scaffolds were immersed in 50 ml of distilled water for 28 days at 37 °C in accordance with previous study (Li et al. 2010). The distilled water was changed for a time period at day 1, 6, 7, 7, and 7. The supernatants were collected. The collected supernatants were filtered by using 0.2 μm syringe filter. The filtered supernatants were analyzed for Si, Ca, Na, and P ions. The concentrations of each ion released from scaffold were measured by inductively coupled plasma optical emission spectrometer (ICP-OES; ICP Optima 8300, Perkin Elmer, Waltham, MA, USA).

Figure 14. Photograph of inductively coupled plasma optical emission spectrometer (ICP-OES; ICP Optima 8300, Perkin Elmer, Waltham, MA, USA).

4. *In vitro* biological properties of HPB scaffold

4.1. Cell culture and culture conditions

Murine pre-osteoblasts (MC3T3-E1; CRL-2693, subclone 4, American Type Culture Collection, Manassas, VA, USA) and murine fibroblast cells (L929; 10001, Korea cell line bank, Seoul, Korea) were used in this study. Cells were cultured in a 100 Φ culture dish and culture media used RPMI 1640 (Welgene, Daegu, Korea) and alpha-modified minimum essential medium (alpha-MEM; Gibco/ ThermoFisher Scientific, Waltham, MA, USA) supplemented with 10 % fetal bovine serum (FBS; Gibco/ThermoFisher Scientific, Waltham, MA, USA) and 1% of antibiotics (penicillin/streptomycin, Gibco/ThermoFisher Scientific, Waltham, MA, USA) was added to the media. The cell culture was supplemented with osteogenic medium (OM; alpha-MEM, 50 μg/mL L-ascorbic acid, 10 mM β-glycerol phosphate, and 100 nM dexamethasone (Sigma Aldrich, St. Louis, MO, USA).

4.2. Cytotoxicity evaluation

Each groups of HAp and HPB scaffolds was immersed in alpha-MEM (100 mg/mL) at 37°C for 24 h and polyethylene film (3 cm^2/mL) was used as control group in accordance with ISO 10993-12 and ISO 10993-5(10993-5 ; I 2009; ISO 2009). Each of MC3T3-E1 cells and L929 cells were dispensed into a 96-well culture plate at a density of 1×10^4 cells/well and allowed to attach overnight. The existing each of alpha MEM and RPMI 1640 was replaced with the prepared extracts and incubated for 24 h. Following removal of extracts, colorimetric 3-(4,5-dimethyltriazol-2-yl)-2,5-diphenylteterazolum bromide (MTT; Sigma Aldrich, St.Louis, MO, USA) reagent was added, followed by incubated for 4 h. After removing the MTT reagent, dimethyl sulfoxide (Sigma Aldrich, St.Louis, MO, USA) was then added, and the plate was shaken for 15 minutes. The absorbance was measured at 570 nm using microplate reader spectrophotometer (Molecular Devices, VersaMax tunable, Sunnyvale, CA, USA).

4.3. Cell proliferation and viability

Cell proliferation was analyzed using a CyQUANT® cell proliferation assay kit (ThermoFisher Scientific, Waltham, MA, USA), and the assay was performed according to the manufacturer's protocol. Briefly, the cells with scaffolds were cultured for 1 and 3 days. The scaffolds were washed with PBS, and the adherent cells were detached and suspended by treatment with trypsin. The prepared cell suspension with cell-lysis buffer was centrifuged for 5 minutes at 2,000 rpm, and the supernatant was carefully removed. The CyQUANT® GR dye was added in the cell pellet, and the cells were re-suspended by brief vortexing. The cells were transferred to a black 96-well plate, and they were analyzed using a FlexStation III microplate reader (Molecular Devices) with a fluorescence mode at Ex/Em = 480/520 nm.

The viability of the cells on the scaffold was analyzed using the LIVE/DEAD™ Viability/Cytotoxicity Kit for mammalian cells (ThermoFisher Scientific, Waltham, MA, USA). Briefly, scaffolds seeded with cells were incubated during 7 days and washed with PBS. The cells on the scaffold were then stained in LIVE/DEAD reagents for 30 min. The HPB scaffolds were then observed by confocal laser scanning microscope (LSM 700, Zeiss, Oberkochen, Germany) to assess viability of the cells on the scaffold.

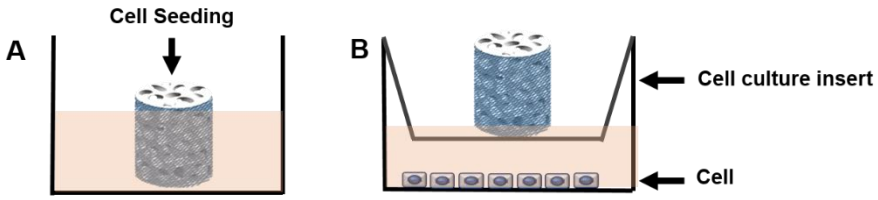

Figure 15. Schematic diagram of cell culture experiments. (A) Direct contract method (B) Indirect contact method.

Figure 16. Photograph of confocal laser microscopy (LSM700, Carl Zeiss, Oberkochen, Germany).

4.4. Alkaline phosphatase activity

Alkaline phosphatase (ALP) activity in preosteoblast MC3T3-E1 was measured by spectrophotometric analysis using the Sensolyte® p-Nitrophenyl phosphate (pNPP) ALP assay kit (AnaSpec, San Jose, CA, USA) at day 3 and 7, and the procedure was followed its protocol. Briefly, cells were seeded at a density of 1×10^5 cells/ well with each groups of scaffolds in cell insert. Each groups of scaffolds in the cell insert were removed in the 6-well plate. The cells were rinsed twice with phosphate buffer saline (PBS; Gibco, Grand Island, NY, USA), and were lysed using the 0.2% Triton X-100 (Sigma Aldrich, St. Louis, MO, USA). The lysate was incubated at 4 °C for 10 minutes under agitation, and the cell suspension was centrifuged at 2,500 ×g for 15 min at 4 °C. 50 μL of supernatant was added into each 96-well plate, and 50 μL of pNPP substrate solution was added into each 96-well plate. The reagent was mixed by gently shaking for 30 seconds, and the absorbance was determined at 405 nm after 1 hours.

The total protein was quantified by the Bradford protein assay kit (ThermoFisher Scientific, Waltham, MA, USA) in accordance with the manufacturer's protocol. Briefly, each groups of scaffolds in the cell insert were removed in the 6-well plate. The cells were rinsed twice with PBS. The supernatant from lysate were prepared above and the 10 μL of supernatant was placed into a microplate well. The 300 μL of the working solution from the assay kit was placed into each plate and mixed on a plate shaker for 30 seconds followed by incubating plate for 10 minutes at room temperature. The absorbance was measured with 595 nm on a microplate reader.

4.5. Western blot analysis

To examine the stage of osteogenic differentiation for demonstrating osteopontin expression, western blot was observed at 7 and 14 days. Briefly, cells were seeded at a density of 1×10^5 cells/ well with each groups of scaffolds in cell insert. Each groups of scaffolds in the cell insert were removed in the 6-well plate. The cells were harvested in lysis buffer. After sonication, the samples were centrifuged for 5 min at 13,000 rpm. The quantification of protein contents was performed by protein extraction for Bradford method (PRO-PREP, iNtRon Biotechnology, Seongnam, Korea). The prepared proteins of each group were separated on sodium dodecyl sulphate-polyacrylamide gel (4 and 15%) electrophoresis. After electrophoresis, the proteins were transferred to polyvinylidene difluoride membrane (Millipore, Schwalbach, Germany), and the blots were subsequently probed with the anti-OPN antibody (ab11503, Cambridge, UK). For detection, horseradish peroxidase-conjugated secondary antibody (Santa Cruz, CA, USA) was used. Normalization of results was ensured by running parallel western blots with anti-glyceraldehyde dehydrogenase (GAPDH) antibody (ab8245, Cambridge, UK).

4.6. Immunocytochemistry

To examine the stage of osteogenic differentiation for demonstrating COL-I, RUNX2, and OPN, the immunocytochemistry (ICC) staining was performed to detect specific expression patterns exhibited by proteins. The primary antibodies were used with COL-I (ab34710, Cambridge, UK), RUNX2 (ab76956, Cambridge, UK), and OPN (ab11503, Cambridge, UK) to identify osteogenic differentiation. In details, cells cultured on the scaffolds were fixed in 4% paraformaldehyde on day 7 and 14, permeabilized with 0.2% Triton X-100 in PBS and then blocked in 10% normal donkey serum (ab7475, Cambridge, UK). After blocking, the cells were incubated overnight at 4°C with the primary antibodies targeting the osteoblast specific marker proteins. After washing with PBS, fluorescein isothiocyanate (711-095-152), Cy3 (715-165-151), and Alexa Fluora 647 (705-606-147) conjugated antibodies were added to the cells for an hour and 4',6-diamidino-2-phenylindole (DAPI; ThermoFisher Scientific, Waltham, MA, USA) was used for nuclei staining. Representative fluorescence images of stained cells on the scaffold were obtained using a confocal laser scanning microscope.

4.7. Extracellular mineralization

To demonstrate mineralization of osteogenic differentiation, Alizarin Red Staining (ARS) assay was observed at days 14 and 21. Cells were seeded at a density of 1×10^5 cells/ well with each groups of scaffolds in cell insert. The cell culture was supplemented with OM. Briefly, the cells on the plate with scaffold were washed with PBS and then fixed with ice-cold 70% ethanol for 1 hours. The fixed cells were stained for 40 mM ARS solution pH adjusted to 28% (w/v) ammonium hydroxide (Sigma Aldrich, St Louis, MO, USA) for 10 minutes. After washing out the remaining dye with distil water, the cells were observed under light microscope (IX71/DP71, OLYMPUS, Tokyo, Japan) and representative views were photographed. The quantitative analysis of cells stained ARS were performed by using 10% cetylpyridinium chloride (Sigma Aldrich, St. Louis, MO, USA) in 10 mM sodium phosphate (pH 7.0, Sigma Aldrich, St Louis, MO, USA) for 15 minutes. The absorbance of 100 μL aliquots were transferred to 96-well plate (SPL, Daegu, Korea) and was measured at 562 nm.

5. Statistical analysis

Experimental data were processed with one-way ANOVA followed by Tukey's post-hoc analysis (SPSS, Chicago, IL, United States) to establish statistical significance. Significant difference between each group was determined at $p < 0.05$. Error bars represented the mean ± standard deviation (SD) of measurements.

III. RESULTS

1. Characterization of HPB scaffold

1.1. Surface morphology and elements analysis

The surface morphology and structure of HPB scaffolds observed in SEM (Figure 17). SEM images of HPB scaffold showed micro and macro pore structure (Figure 17A), which was due to irregular sintering at 1250 °C. SEM images showed composite fibers in HPB scaffolds (Figure 17B), where PLGA/BG composite fibers of HPB30 scaffold was the thickest compared to any other groups. HPB10, HPB20, and HPB30 scaffolds showed surface chemistry composition (Figure 17C). Spot 1 is indicated as Si, Ca, Na, and P. Spot 2 is indicated as Ca and P only (without presence of Si or Na). These results showed HPB scaffold generally maintained the components of HAp and 45S5 BG.

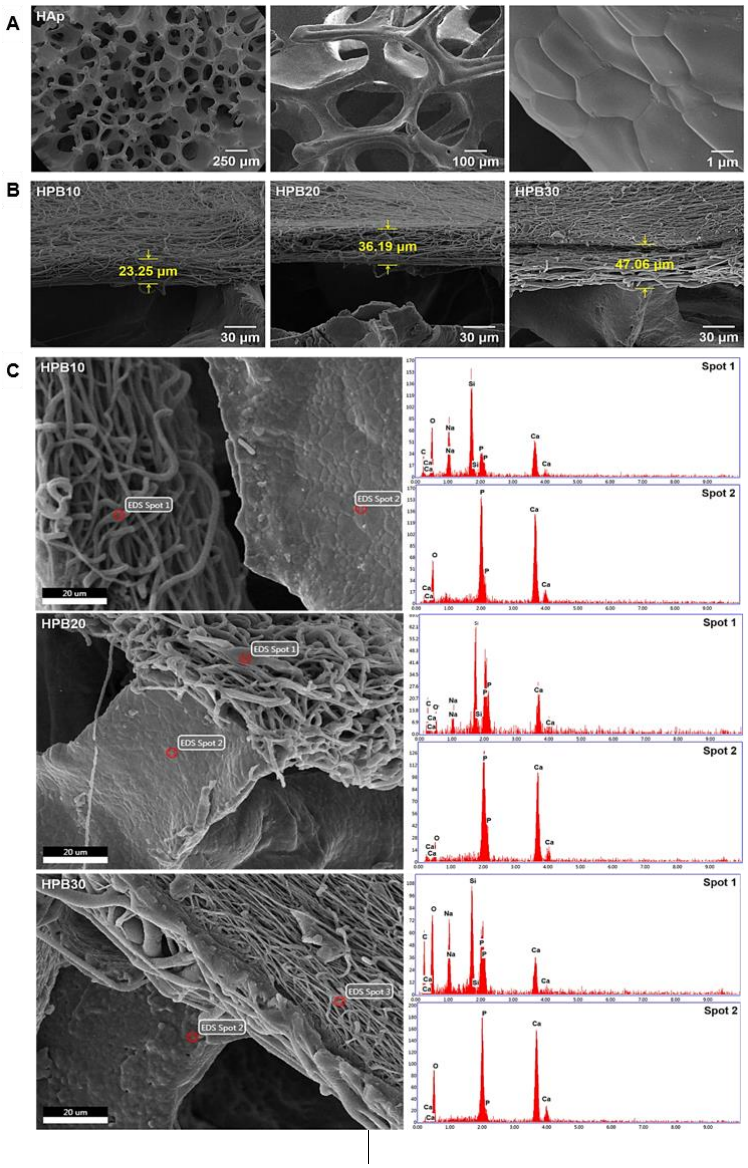

Figure 17. Morphology of the HAp and HPB scaffolds. (A) Representative SEM images of porous HAp scaffolds. (B) Representative SEM image of HPB scaffolds with thickness of 45S5 BG contained PLGA microfibers. (C) SEM-EDS analysis of HPB10, HPB20, and HPB30 scaffolds. They were detected to Ca and P atoms in HAp and Si, Ca, Na and P atoms in 45S5 BG contained PLGA microfiber.

1.2. Micro-computed tomography analysis

The porosity of HPB scaffolds was observed in micro-CT (Figure 18). The HAp component of HPB scaffold had high radiopacity. However, the 45S5 BG/PLGA composite microfibers layer of HPB scaffold had low radiopacity. Hence, HPB scaffold indicated the based on the HAp scaffold structure. The porosity of HPB scaffold was 89 % and it was highly porous structure similar as cancellous bone.

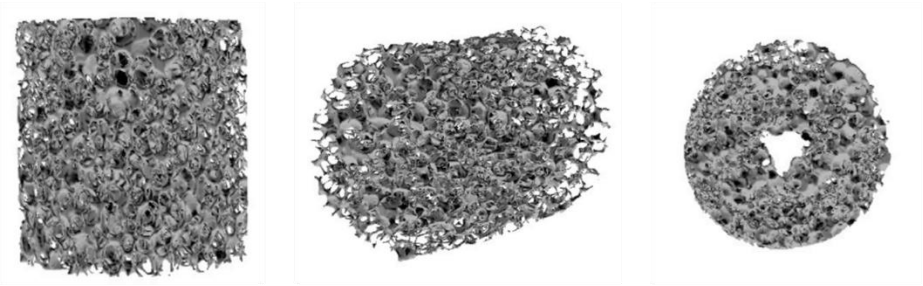

Porosity (%)	Pore size (μm)	Closed porosity (%)	Open porosity (%)
89.064 ± 1.374	695.420 ± 63.507	0.292 ± 0.218	89.031 ± 1.382

Figure 18. The pore properties of HPB scaffold. HPB scaffold was based on the HAp scaffold. HAp scaffold was highly porous structure similar as cancellous bone. This hole was penetrated by using the metallic stick for fabricating the HPB scaffold.

1.3. Thermogravimetric analysis

The TGA pattern of HAp powder, HAp scaffold, 45S5 BG, PLGA at heating rate of 10 °C/min and at temperature up to 500 °C is shown in Figure 19. The results show that HAp and 45S5 BG are no weight loss up to 500 °C but PLGA fibers was weight loss between 200 °C and 400 °C (Figure 19A). The results of TGA patterns for PLGA/45S5 BG composition in the HPB scaffolds showed that PLGA microfiber decreased weight in the temperature range from 100 °C and 300 °C. After removing PLGA microfibers of HPB scaffold below 300 °C, the remaining weight of the 45S5 BG containing PLGA microfibers represents the 45S5 BG particles (Figure 19B). These results indicated the similar values to those of 45S5 BG and PLGA used in actual scaffold fabrication process.

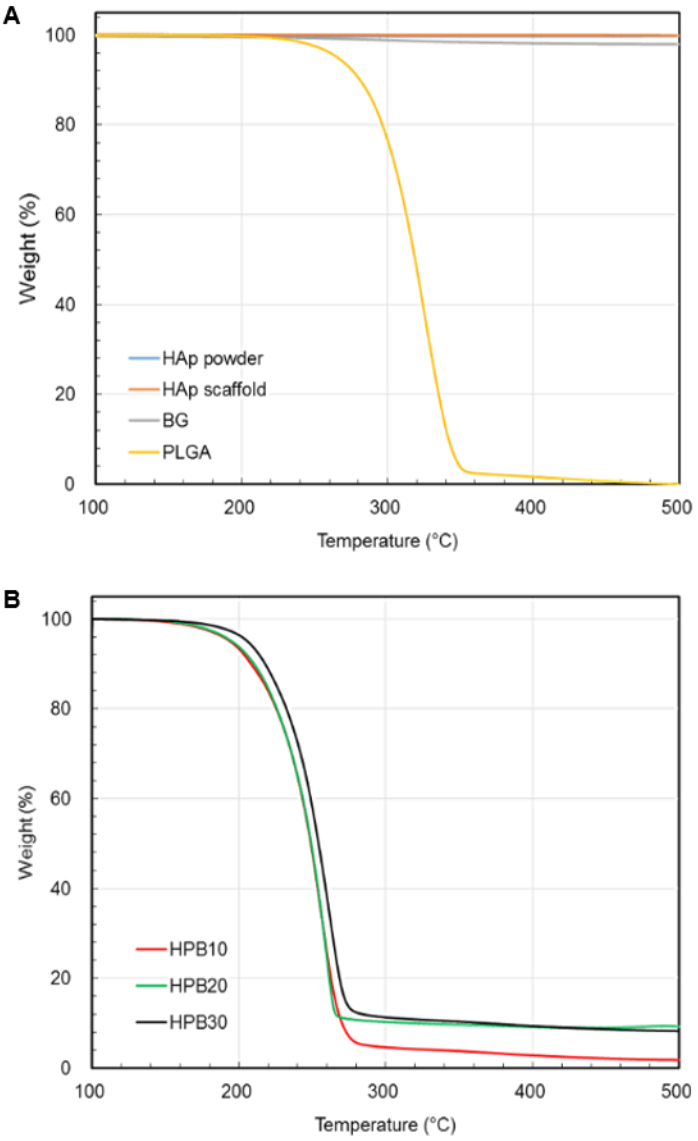

Figure 19. The thermogravimetric analysis (TGA) of PLGA/45S5 BG compositions in the HPB scaffolds. (A) TGA pattern of HAp, 45S5 BG, and PLGA fibers. PLGA fibers were burned between 200 °C and 400 °C (B) TGA pattern of HPB10, HPB20, and HPB30 scaffolds.

1.4. Ion release analysis

In general, the Ca and P ion accumulations increased in all of scaffolds during 28 days, while additional Si and Na ion accumulations were evident on all of scaffolds except HAp (Figure 20 and Table 2). A release of Ca and P ions from each scaffold continually increased into the distilled water during 28 days for all of scaffolds. For Si ion, sharp release of ions from each HPB scaffold into the distilled water was evident during 1 day and 7 days of immersion. However, for HPB10 and HPB20, the release of Si plateaued from 14 days until 28 days whereas constant release was evident with HPB30 scaffold into distilled water during same period. For Na ion, a burst release of Na ions from each HPB scaffold into the distilled water was noticed during 1 day and 7 days of immersion. The release was then plateaued from 7 days until 28 days for HPB10 and HPB20. However, for HPB30, scaffold released Na ions until 14 days, which is then plateaued from 14 days until 28 days. Therefore, the durations of Si, Ca, Na, and P ions release were the longest in the HPB30 scaffold, and the accumulated ions were also the highest in the HPB30 scaffold.

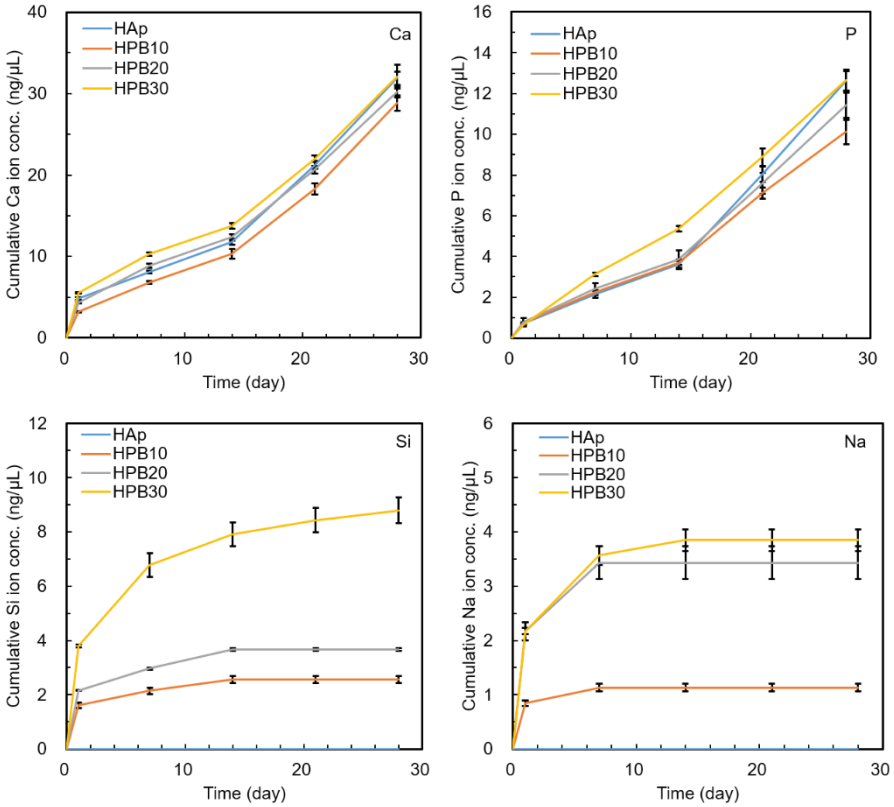

Figure 20. Ion release of HAp and HPB scaffolds into distilled water, represented by cumulative release of Ca, P, Si, and Na ions (n = 3, Si and Na ions are not contained in the HAp scaffold).

Table 2. The cumulative of Ca, P, Si, and Ni ion release of HAp and HPB scaffold for 1 day. The different lowercase letters indicated statistically significant difference between each group in time period ($p < 0.05$).

Unit; ng/μL

Ca	day 1	day 7	day 14	day 21	day 28
HAp	4.838 ± 0.137^{b}	8.086 ± 0.182^{c}	11.800 ± 0.376^{c}	21.232 ± 0.490^{b}	31.873 ± 0.792^{a}
HPB10	3.211 ± 0.085^{d}	6.805 ± 0.159^{d}	10.336 ± 0.588^{d}	18.306 ± 0.670^{d}	28.836 ± 0.957^{c}
HPB20	4.358 ± 0.147^{c}	8.838 ± 0.261^{b}	12.337 ± 0.355^{b}	20.651 ± 0.493^{c}	30.164 ± 0.689^{b}
HPB30	5.506 ± 0.092^{a}	10.301 ± 0.199^{a}	13.738 ± 0.348^{a}	21.981 ± 0.390^{a}	32.087 ± 1.487^{a}

Table 3. The cumulative of P ion release of HAp and HPB scaffold for 28 days. The different lowercase letters indicated statistically significant difference between each group in time period ($p < 0.05$).

Unit; ng/μL

P	day 1	day 7	day 14	day 21	day 28
HAp	0.691 ± 0.028[a]	2.152 ± 0.192[c]	3.620 ± 0.232[c]	8.035 ± 0.374[b]	12.618 ± 0.478[a]
HPB10	0.754 ± 0.035[a]	2.243 ± 0.079[c]	3.684 ± 0.095[c]	7.109 ± 0.271[d]	10.112 ± 0.603[c]
HPB20	0.777 ± 0.209[a]	2.408 ± 0.294[b]	3.873 ± 0.413[b]	7.583 ± 0.514[c]	11.426 ± 0.610[b]
HPB30	0.646 ± 0.057[a]	3.125 ± 0.084[a]	5.356 ± 0.136[a]	8.879 ± 0.435[a]	12.642 ± 0.523[a]

Table 4. The cumulative of Si ion release of HAp and HPB scaffold for 28 days. The different lowercase letters indicated statistically significant difference between each group in time period ($p < 0.05$).

Unit; ng/μL

Si	day 1	day 7	day 14	day 21	day 28
HAp	0.000^{d}	0.000^{d}	0.000^{d}	0.000^{d}	0.000^{d}
HPB10	1.601 ± 0.102^{c}	2.143 ± 0.118^{c}	2.572 ± 0.129^{c}	2.572 ± 0.129^{c}	2.572 ± 0.129^{c}
HPB20	2.153 ± 0.012^{b}	2.965 ± 0.031^{b}	3.666 ± 0.053^{b}	3.666 ± 0.053^{b}	3.666 ± 0.053^{b}
HPB30	3.796 ± 0.046^{a}	6.784 ± 0.433^{a}	7.919 ± 0.438^{a}	8.437 ± 0.447^{a}	8.796 ± 0.481^{a}

Table 5. The cumulative of Na ion release of HAp and HPB scaffold for 28 days. The different lowercase letters indicated statistically significant difference between each group in time period ($p < 0.05$).

Unit; ng/μL

Na	day 1	day 7	day 14	day 21	day 28
HAp	0.000^{d}	0.000^{d}	0.000^{d}	0.000^{d}	0.000^{d}
HPB10	0.842 ± 0.051^{b}	1.129 ± 0.069^{b}	1.129 ± 0.069^{c}	1.129 ± 0.069^{c}	1.129 ± 0.069^{c}
HPB20	2.174 ± 0.167^{a}	3.433 ± 0.306^{a}	3.433 ± 0.306^{b}	3.433 ± 0.306^{b}	3.433 ± 0.306^{b}
HPB30	2.171 ± 0.056^{a}	3.569 ± 0.174^{a}	3.848 ± 0.196^{a}	3.848 ± 0.196^{a}	3.848 ± 0.196^{a}

2. *In vitro* biological properties of HPB scaffold

2.1. Cytotoxicity evaluation

The cytotoxicity of HAp and HPB scaffold showed in Figure 21. The relative cell viability used MC3T3-E1 cells on HPB30 scaffold was significantly lower than that of the control group ($p < 0.05$). However, there was no significant difference in the relative cell viabilities between HAp and all HPB scaffolds. In addition, the relative cell viability used L929 cells was no significant difference between HAp and all HPB scaffolds.

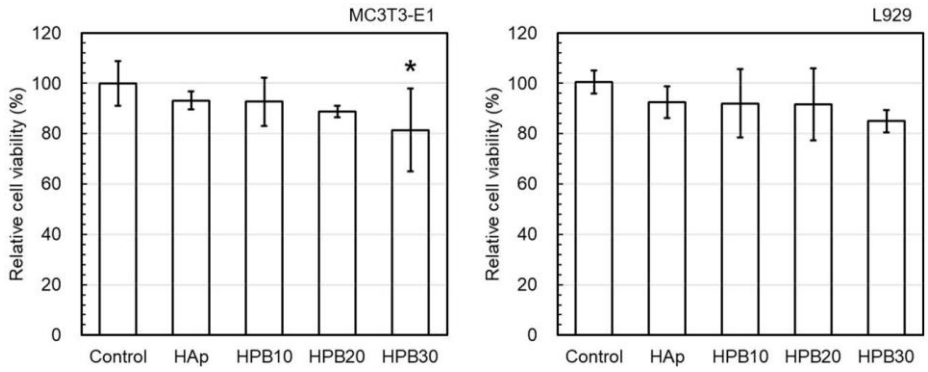

Figure 21. The cytotoxicity of HAp and all HPB scaffold in both MC3T3-E1 and L929 cells. (n = 5; *; $p < 0.05$, statistically significant differences compared to control group).

2.2. Cell proliferation

The proliferation results of MC3T3-E1 cells on HAp and HPB scaffolds showed in Figure 22. Cell proliferation on the HPB30 scaffold was significantly lower than HAp, HPB10, and HPB20 on day 1 ($p < 0.001$). Whereas, cell proliferation on the HPB30 scaffold was significantly lower than that of HAp and HPB10 ($p < 0.001$). Only HPB10 in the HPB groups showed higher cell proliferation than HAp.

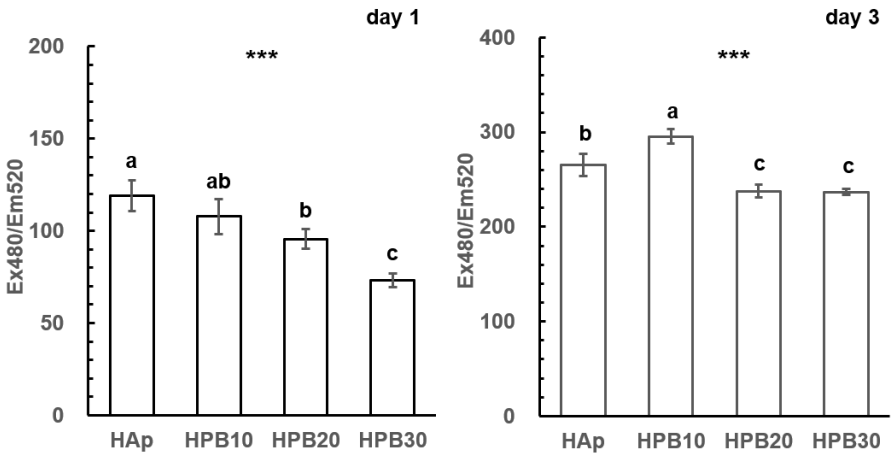

Figure 22. Cell proliferation of HAp and all HPB scaffolds. Cell proliferation revealed that cells had good viability within all groups ($n = 5$, ***; $p < 0.001$). The different lowercase letters indicated statistically significant difference ($p < 0.05$).

2.3. Cell viability

The viability results of MC3T3-E1 cells on HAp and HPB scaffolds showed in Figure 23. These results confirmed with LIVE/DEAD staining, where green fluorescence indicated live cells and red fluorescence indicated dead cells. There was no obvious difference in the number of red cells on each scaffold. However, most cells were alive with green fluorescence. Cells were present on the HAp scaffold but for HPB scaffolds, they were also attached to the PLGA/BG composite microfibers.

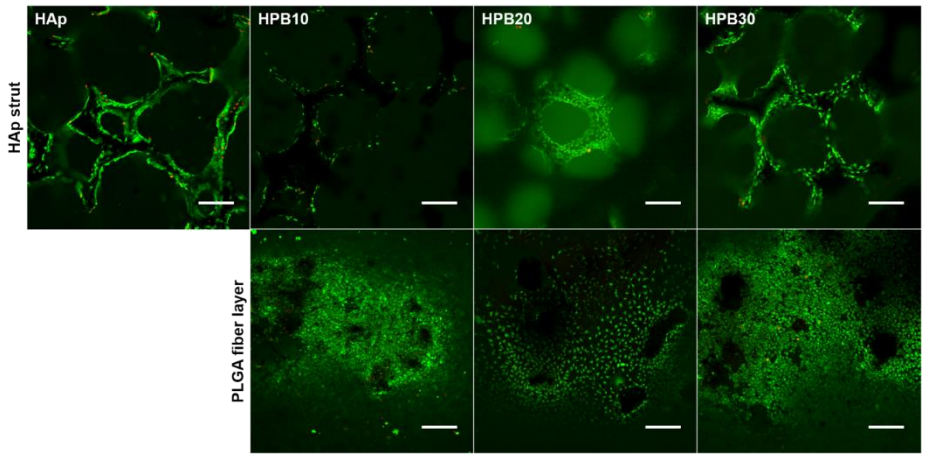

Figure 23. LIVE/DEAD staining of the HAp and HPB scaffolds after 7 days. Cells on the HAp structure and 45S5 BG contained PLGA microfibers layer (scale bar = 200 μm).

2.4. Alkaline phosphatase activity

ALP activity results of MC3T3-E1 cells on HAp and HPB scaffolds showed in Figure 24. On day 3, ALP activity of HPB30 scaffold was lower than that of HAp, HPB10, and HPB20 scaffold ($p < 0.01$) although there was no statistically significant difference between HAp and HPB10 scaffold ($p > 0.05$). However, on day 7, ALP activity of HPB 30 scaffold was higher than those of HAp and HPB10 scaffold ($p < 0.001$) although there was no statistically significant difference between HPB20 and HPB30 scaffold ($p > 0.05$)

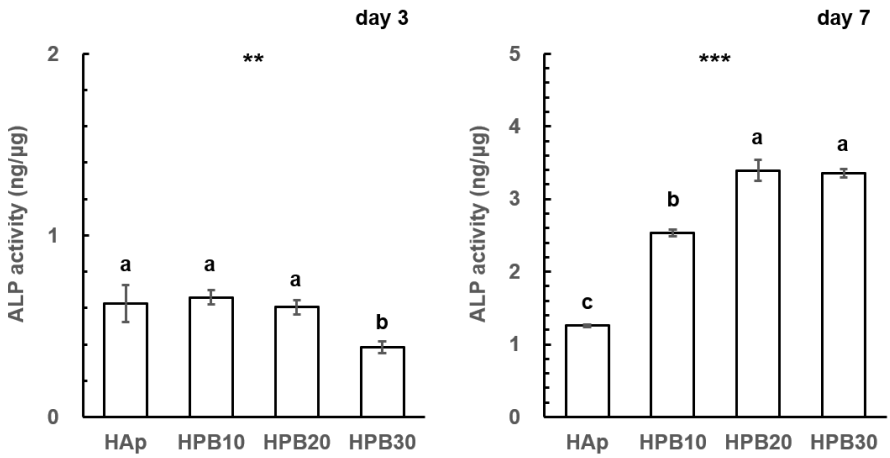

Figure 24. ALP expression (normalized by DNA in sample) of MC3T3-E1 within HAp and HPB scaffolds after 3 and 7 days. Osteoinductivity of HAp and HPB scaffolds *in vitro*. ($n = 3$, **; $p < 0.01$ and ***; $p < 0.001$). The different lowercase letters indicated statistically significant difference ($p < 0.05$).

2.5. Western blot analysis

Osteopotnin expression results of MC3T3-E1 cells on HAp and HPB scaffolds showed in Figure 25. There was no statistically significant difference between HAp and all HPB scaffold at 1 week ($p > 0.05$). Whereas, osteopontin expression result of HPB30 scaffold was higher than that of HAp, HPB10, and HPB20 scaffold ($p < 0.001$) at 2 weeks although there was no statistically significant difference between HAp and HPB10 scaffold ($p > 0.05$).

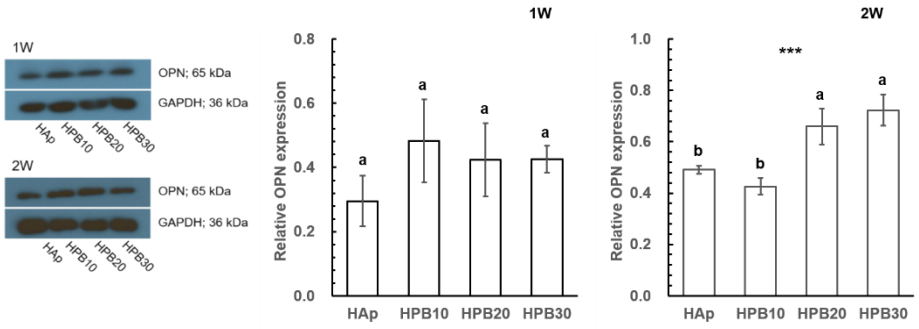

Figure 25. Osteogenic expression levels of OPN normalized to GAPDH ($n = 3$, ***; $p < 0.001$). The different lowercase letters indicated statistically significant difference ($p < 0.05$).

2.6. Immunocytochemistry

Osteogenic activity results of MC3T3-E1 cells on HAp and HPB scaffolds showed in Figure 26. To further consider osteogenic properties of the HAp and all HPB scaffold, ICC analyses were carried out for COL-I, RUNX2, and OPN with MC3T3-E1 cells cultured on HAp and HPB scaffolds for 7 and 14 days. First of all, osteogenic activity was detected for MC3T3-E1 on both 7 and 14 days. HAp and HPB scaffold tend to show similar level of COL-I and RUNX2 expression. However, expression of OPN level was only evident with MC3T3-E1 cells on HPB scaffolds and absent on HAp scaffold, on both 7 and 14 days.

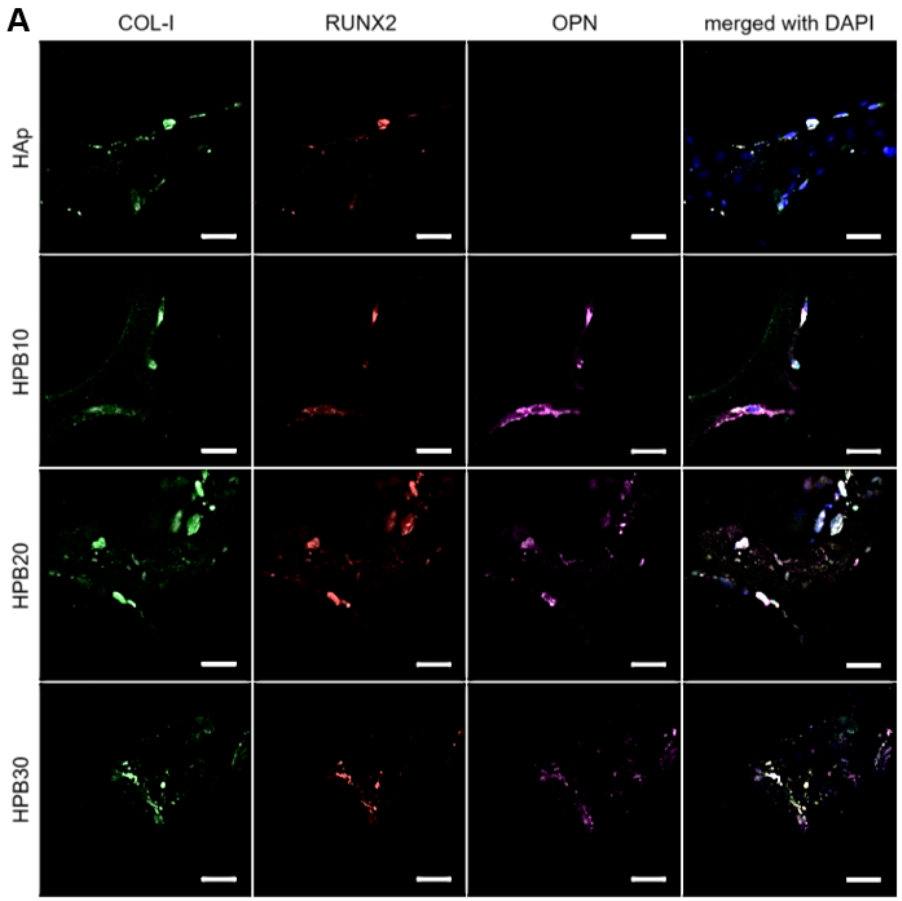

Figure 26. Osteogenic activity of MC3T3-E1 cells cultured on HAp and HPB scaffold as indicated by ICC of osteogenic protein expression level (COL-I, RUNX2, and OPN) following culture for (A) 7 and (B) 14 days (scale bar = 20 μm) (To be continued next page).

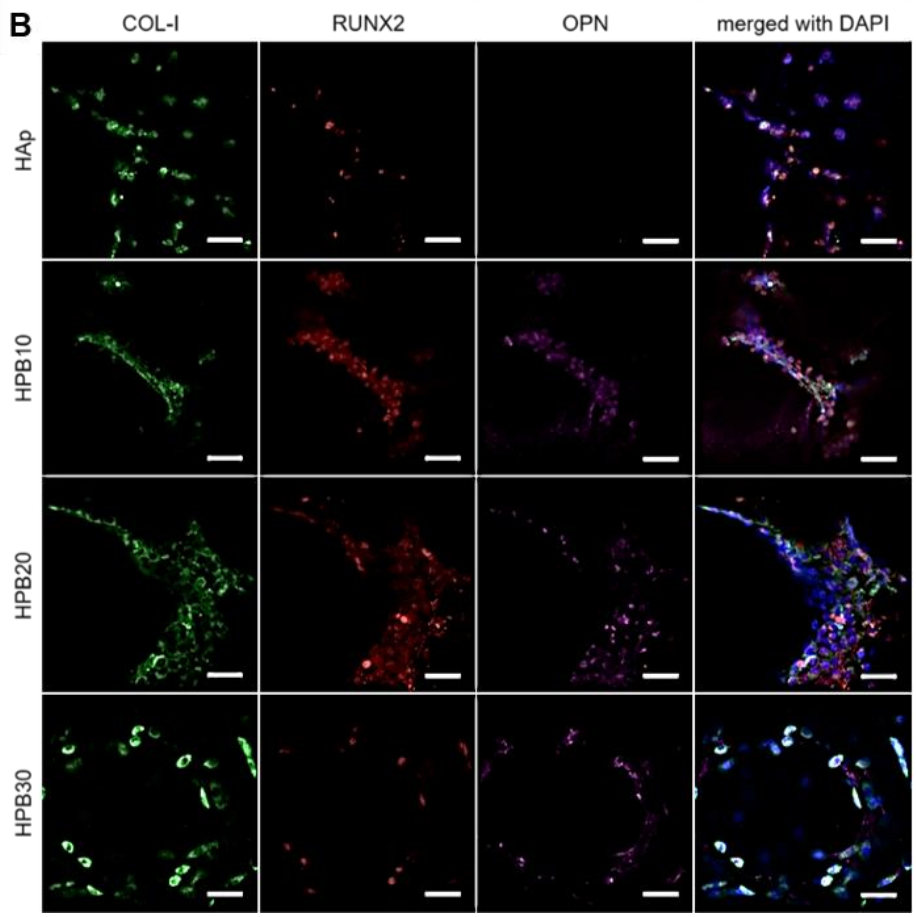

2.7. Extracellular mineralization

To examine the later stage of osteogenic differentiation, ARS was observed in 14 and 21 days as shown in Figure 24. It was first identified that there was no evidence of bone mineralization on all of groups following 14 days of culture and both of the control group (only MC3T3-E1 cells) and HAp group. Whereas, extracellular mineralization showed to occur on 21 days for HPB10 scaffold as evident by red coloration. Extracellular mineralization of HPB20 and HPB30 scaffold were significantly greater than those of control, HAp, and HPB10 scaffold on 21 days. The quantitative analysis of the ARS showed that all HPB scaffold was statistically lower than HAp scaffold on 14 days ($p < 0.001$). However, the quantitative analysis of the ARS showed that HPB30 scaffold was statistically higher than control, HAp, HPB10, and HPB20 scaffold on 21 days ($p < 0.001$).

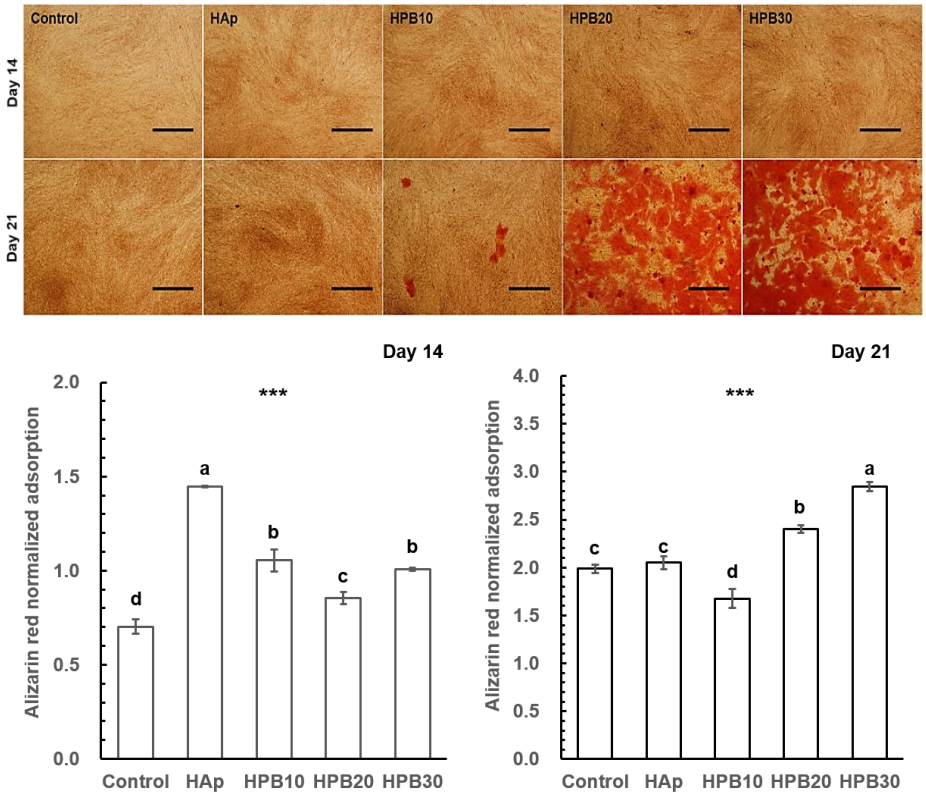

Figure 27. Mineralization of MC3T3-E1 cells by ions released from HPB scaffolds during 14 and 21 days (scale bar; 1 mm) ($n = 3$, control; only MC3T3-E1 cells, ***; $p < 0.001$). The different lowercase letters indicated significant difference ($p < 0.05$).

IV. DISCUSSION

HAp is a widely used material for osteoconduction because of its high biocompatibility and ability to obtain a porous bone like structure (Hong et al. 2014b). However, the limitation of the material lies in the lack of characteristics such as osteoinduction, which is required for filling in the defect sites of bone that would assist osteoblasts in the repair process. On the other hand, 45S5 BG promotes a higher level of osteoinduction and osteoconduction in bone defects (Rahaman et al. 2011). The difference is due to the release of ions from each material. 45S5 BG continuously release a greater amount of ions than HAp in physiological conditions. However, HAp is mainly composed of calcium and phosphate, whereas 45S5 BG mainly consists of Si, meaning that these two bone-substitute materials are different in crystal or amorphous structure. In this sense, it is reasonable to conclude that these two materials might have separate roles in maintaining osteoblasts in bone defects. Thus, we raised the question whether HAp and 45S5 BG coexist in human bone tissue within a bone defect area. In order to solve the question, PLGA microfibers were applied to coexisting HAp and 45S5 BG. 45S5 BG was loaded into the microfiber layer, which was made with PLGA which was component of lactide and glycolide ratio of 65:35. The PLGA 6535 containing drugs or metallic ions displayed the longest acting effects compared PLGA which was lactide and glycolide ratio of 50:50 (Anderson and Shive 1997). Considering the period of *in vitro* tests, PLGA having a ratio exceeding lactide and glycolide ratio of 65:35 was not selected. Based on the HAp, 45S5, and PLGA microfibers, this study hypothesized that the scaffold consisting of 45S5 BG-loaded PLGA microfibers coated on the sidewall of the HAp scaffold might play a significant role in promoting bone growth and regeneration.

In this study, HPB scaffolds confirmed that it maintained the porous structure of HAp scaffolds, whereas the other component is composed of 45S5

BG/PLGA microfibers (Figure 17). The pore size of porous scaffolds ranged from 200 to 500 μm. In addition, The porosity of HPB scaffold was 80 – 90% (Figure 18), respectively, which were similar to those of cancellous bone like structure and therefore would provide effective cell proliferation and differentiation (Loh and Choong 2013). On the contrary, the composite electrospun microfibers of HPB scaffolds had pore sizes that were smaller than those of the porous HAp scaffold. However, the electrospun microfibers of the HPB scaffolds provided the specific surface area for cell adhesion. In previous studies, electrospun microfibers were indicated to be effective for cell attachment (Hong et al. 2018). HPB scaffold confirmed that the electrospun microfiber thickness was increased with time but it was not increased proportionally. When fabricating the electrospun microfibers, electrospun microfibers was not immediately changed to solid state. The solvent in the solution jet needs to have sufficient time to evaporate and turn the jets into dry microfibers (Robb and Lennox 2011).

HPB scaffolds were performed to confirm the components of HAp and 45S5 BG (Figure 17C). HPB scaffolds were observed that 45S5 BG was in a pure state in the composite microfibers, which were combined with the HAp scaffold. Previously, HAp and 45S5 BG were detected in pure states in fibrous composite scaffolds (Jose et al. 2009; Luo et al. 2017). In addition, PLGA and 45S5 BG composite microfibers of HPB scaffolds were quantitatively analyzed (Figure 19). HPB20 and HPB30 scaffold had the same ratio of PLGA to 45S5 BG when compared to their composite solution state. However, HPB10 had a lower ratio of PLGA to 45S5 BG than HPB20 and HPB30. Therefore, by comparing the ratio at PLGA to 45S5 BG ratio, it demonstrated that short electrospinning time is not effective for the fabrication of electrospun 45S5 BG-containing PLGA microfibers.

HAp and HPB scaffolds were compared in terms of their cytotoxicity (Figure 21) and cell proliferation rate (Figure 22). The evaluation showed an absence of cytotoxicity in the HPB scaffolds. Notably, lactic acid caused toxicity by biodegradation of PLGA. However, the components of the HPB scaffolds, HAp and 45S5 BG ions, neutralized the lactic acid. According to Vergnol et al, the released ions from 45S5 BG enable cells to dwell in the poly(lactic acid)(PLA). The degradation of PLA may, in turn, easily cause cell death because of changes in pH. Both polymeric and ceramic composite materials demonstrated an absence of cytotoxicity (Vergnol et al. 2016). When cells were seeded on the surface of the HAp and HPB scaffolds, we observed that the cells adhered and proliferated. The HAp structure and the PLGA/45S5BG composite electrospun microfibers in the HPB scaffolds affected the attachment of the cells. According to Hong et al., MC3T3-E1 cells were attached of osteoblasts and imaging of three-dimensional cell growth (Hong et al. 2014a). In addition, PLGA composite fibers at the sidewall of the HPB scaffolds showed increased cell attachment compared to those on the HAp scaffold. The specific surface area of the HPB scaffolds increased more than that of the HAp scaffold with the SEM images in this study. It was previously reported that electrospun PLGA microfibers enhanced the attachment of osteoblasts and imaging of three-dimensional cell growths (Hong et al. 2018).

According to the results of inductively coupled plasma optical emission spectroscopy (ICP-OES) (Figure 20), Ca and P ions were continuously released in HAp and HPB scaffolds. Based on the component of nano HAp in the HAp and HPB scaffold, nano HAp had high solubility and in consequence high resorption rate in compared with pure stoichiometric HAp (Higuchi et al. 2019; Mocanu et al. 2021). Meanwhile, Si and Na ions were quickly released in comparison to Ca and P ions, possibly because of the accelerated degradation of 45S5 BG. The release kinetics of 45S5 BG in PLGA electrospun microfibers could be easily controlled by regulating the Si-Ca-Na-P ions (Table 2). 45S5

BG has shown improved osteogenesis since first reported by Hench (Hench 2009). In the present study, we demonstrated that the released Si ions from PLGA/45S5 BG composite electrospun microfibers on the HPB scaffolds were important for stimulating osteogenesis. Some studies have reported that Si ions released from 45S5 BG enhanced osteogenesis (Gough, Jones, and Hench 2004; Sun et al. 2007; Wu et al. 2011). Also, 45S5 BG released Ca and P ions persistently, which improved osteoblastic differentiation (Hoppe, Güldal, and Boccaccini 2011).

HAp and 45S5 BG could enhance the osteogenic activity of MC3T3-E1, as indicated by cells on the HPB scaffolds compared to those on the HAp scaffold. The HPB30 scaffold showed that ALP activity, which is marker of early osteogenic differentiation, has the tendency to dramatically increase (Figure 24). Tsigkou et al. reported that culture medium without 45S5 BG ions (Tsigkou et al. 2009). In addition, Rath et al. reported that 45S5 BG stimulated high amounts of ALP at an earlier time in adipose stem cells and mesenchymal stem cells (Rath et al. 2016).

The HPB30 scaffold significantly promoted osteogenic differentiation by enhancing the expression of bone-related genes (Figure 25). The HPB30 scaffold induced the protein expression of osteopontin in MC3T3-E1. 45S5 BG significantly enhanced the osteoinductive capacity of the HPB scaffolds, which is critical for bone repair and regeneration (Ajita, Saravanan, and Selvamurugan 2015). In this experiment, the ICC analysis suggested that the BG in HPB scaffolds stimulated the upregulation of three genes (COL-I, RUNX2, and OPN) associated with the process of osteogenic differentiation (Figure 26). RUNX2 has been identified as the major transcription factor controlling osteogenic differentiation from the preosteoblastic to osteoblastic stage. The expression levels of late differentiation marker genes COL-I and OPN were upregulated by RUNX2 (Komori 2006). Hence, RUNX2 can activate osteoblast-related

gene expression. OPN is a substantial component of the bone matrix and is thought to be responsible for cell attachment to the electrospun microfibers (Zhou et al. 2017). Earlier research indicated that osteogenic differentiation marker genes were stimulated and increased in response to 45S5 BG (Moorthi et al. 2012; Moorthi et al. 2013).

Osteogenic differentiation was further confirmed by evaluating Ca deposition via alizarin red staining in response to HPB30 scaffold treatment with preosteoblast after 21 days (Figure 27). Increased Ca deposition was observed in response to HPB scaffolds along with an environment that stimulated osteogenesis. Notably, Si ions released by 45S5 BG ions played a role in osteoblast function (Dashnyam et al. 2017). The ability of Si ions to produce cell mineralization and nodules in important for the development of appropriate materials for bone repair (Shie, Ding, and Chang 2011). Some studies have found that bone nodules were formed in the presence of 45S5 BG or extracted medium from 45S5 BG ions (Gough, Jones, and Hench 2004; Tsigkou et al. 2009). Hence, it is suggested that HPB scaffolds induce the promotion of osteoblastic environment.

Bone remodeling is based on the concerted action of resorptive and formative cell populations in order to replace old bone with new bone. Resorption is an active process that is mediated by cells showing resorptive activity such as macrophages or osteoclasts. On the other hand, Formation is an active process that is mediated by osteoblasts showing formative activity such as osteoid matrix and osteoid mineralization (Hadjidakis and Androulakis 2006; Raggatt and Partridge 2010). In terms of bone remodeling, although HAp had phagocytosed and degradation by the osteoclasts, HAp was slowly resorbed in the body considering to the physiological environments. Previously, *in vivo* studies demonstrated that HAp had slow biodegradable rate and its property caused to have slowly the new bone formation (Friederichs et al. 2015;

Habibovic et al. 2008; Itoh et al. 2006). Furthermore, HAp was usually maintained more than 3 years after implantation in the body, allowing a slow bone ingrowth progress and cell colonization (Daculsi 1998; Koshino et al. 2001). On the other hand, 45S5 BG had resorption in the physiological environment. Previously, *in vivo* studies demonstrated that 45S5 BG had resorption rate that was in agreement with the bone formation rate and it integrated to bond to the surrounding hard and soft tissue (Bi et al. 2012; Livingston, Ducheyne, and Garino 2002). Furthermore, 45S5 BG had resorption in 6 months considering the clinical environment and tend to have new bone formation and remodeling process (Moimas et al. 2006).

This study had limitation *in vitro* studies that did not consider the clinical outcomes of using HPB scaffold. However, the study clearly showed possibilities of using the HPB30 scaffolds for improved osteogenesis. Based on the *in vitro* studies, HPB30 scaffold could be considered to perform the animal model (e.g. calvaria defect, femur defect) a part of future studies.

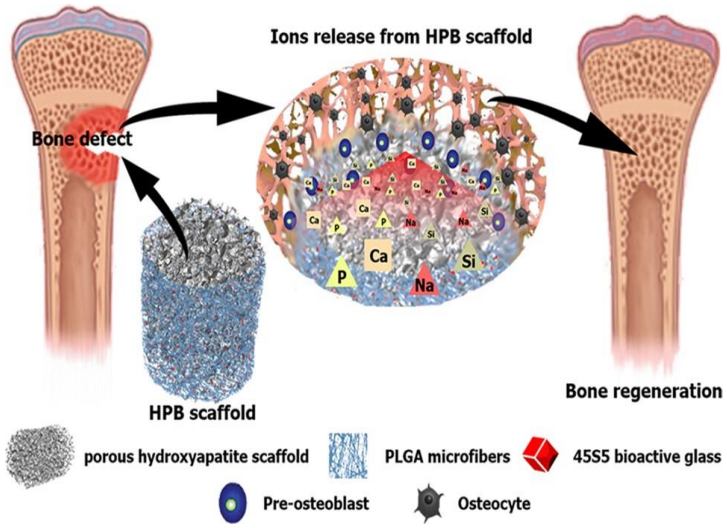

Figure 28. Schematic illustration of osteogenic effects on HPB scaffold in this study.

V. CONCLUSION

Within the limitation of this study, we demonstrated the following:

1. In this study, the HPB scaffold was successfully fabricated by sponge replica and electrospinning methods. Components of HAp in the HPB scaffold were detected through Ca and P atoms. Meanwhile, the components of 45S5 BG in the HPB scaffold were detected through Si, Ca, Na, and P atoms.

2. Si, Ca, Na, and P ions were released from the HPB scaffold. The release of Ca and P ions was observed from the HPB scaffold for 28 days. Additionally, the release of Na and Si ions was observed from the HPB scaffold for 28 days. Si and Na ions of HPB30 scaffold were released longer than those of HPB10 and HPB20 scaffolds.

3. In terms of Si ion-release from HPB scaffold, HPB scaffold had the effectiveness of the osteogenic differentiation in the pre-osteoblasts. The osteogenic effect of HPB30 scaffold was greater than that of HPB10 and HPB20 scaffolds.

In terms of the initial hypothesis of this study, components of HPB scaffold indicated Si, Ca, Na, and P atoms. However, components of HAp scaffold indicated only Ca and P atoms. Thus, the first null hypothesis was partially accepted. In terms of the second null hypothesis of this study, HPB scaffolds confirmed to release Si, Ca, Na, and P ions. However, HAp scaffold confirmed to release only Ca and P ions. Correspondingly, the second null hypothesis was partially accepted. HPB scaffolds enhanced the osteogenic effect in comparison with HAp scaffold and there are significantly difference *in vitro*. Therefore, the third null hypothesis was rejected.

Overall, HPB scaffolds prepared by the two-step fabrication method as

described in this research are promising materials for critical bone regeneration. HPB scaffolds will be useful for the treatment of bone defects as HAp and 45S5 BG are suitable as biomaterials for the human bone. HPB scaffolds not only have cancellous bone-like structure but also are able to support cell migration, allowing the growth of MC3T3-E1. Most importantly, it can be observed that four types (Si-Ca-Na-P) of ions are released from the HPB scaffolds, which was shown to be effective in osteogenesis and bone mineralization compared to the HAp scaffold. Based on this study, amongst four types (Si-Ca-Na-P) of ions, Si ion was indicated to stimulate bone repair. Taken together, HPB scaffolds can act as a bone substitute to support the restoration of bone structure and efficient function of damaged bone.

VI. REFERENCES

10993–5: Biological evaluation of medical devices—Part 5: Tests for in vitro cytotoxicity. *ISO*, 2009.

10993-12: 2012 Biological Evaluation of Medical Devices—Part 12: Sample Preparation and Reference Materials. *ISO*, 2012.

Ajita J, Saravanan S, Selvamurugan N: Effect of size of bioactive glass nanoparticles on mesenchymal stem cell proliferation for dental and orthopedic applications. *Mater Sci Eng C* 53: 142-149, 2015.

Albrektsson T, Johansson C: Osteoinduction, osteoconduction and osseointegration. *Eur Spine J* 10(2): S96-S101, 2001.

Anand P, Nair HB, Sung B, Kunnumakkara AB, Yadav VR, Tekmal RR, et al.: RETRACTED: Design of curcumin-loaded PLGA nanoparticles formulation with enhanced cellular uptake, and increased bioactivity in vitro and superior bioavailability *in vivo*. *Biochem Pharmacol* 79(3): 330-338, 2010.

Anderson JM, Shive MS: Biodegradation and biocompatibility of PLA and PLGA microspheres. *Adv Drug Deliv Rev* 28(1): 5-24, 1997.

Arnett TR, Orriss IR: Metabolic properties of the osteoclast. *Bone* 115: 25-30, 2018.

Arora M, Chan EK, Gupta S, Diwan AD: Polymethylmethacrylate bone cements and additives: A review of the literature. *World J Orthop* 4(2): 67-74, 2013.

Baino F, Hamzehlou S, Kargozar SJJofb: Bioactive glasses: where are we and where are we going? *J Funct Biomater* 9(1): 25-50, 2018.

Baldwin P, Li DJ, Auston DA, Mir HS, Yoon RS, Koval KJ: Autograft, allograft, and bone graft substitutes: clinical evidence and indications for use in the setting of orthopaedic trauma surgery. *J Orthop Trauma* 33(4):203-213, 2019.

Bellucci D, Sola A, Anesi A, Salvatori R, Chiarini L, Cannillo V: Bioactive glass/hydroxyapatite composites: Mechanical properties and biological evaluation. *Mater Sci Eng C* 51: 196-205, 2015.

Bi L, Jung S, Day D, Neidig K, Dusevich V, Eick D, et al.: Evaluation of bone regeneration, angiogenesis, and hydroxyapatite conversion in critical-sized rat calvarial defects implanted with bioactive glass scaffolds. *J Biomed Mater Res A* 100(12): 3267-3275, 2012.

Bilgiç E, Boyacıoğlu Ö, Gizer M, Korkusuz P, Korkusuz F: Architecture of bone tissue and its adaptation to pathological conditions. In *Comparative Kinesiology of the Human Body*. Elsevier. 71-90, 2020.

Bohner M: Resorbable biomaterials as bone graft substitutes. *Mater Today* 13(1-2): 24-30, 2010.

Bonewald LF: Osteocytes as dynamic multifunctional cells. *Ann N Y Acad Sci* 1116(1): 281-290, 2007.

Boonrungsiman S, Gentleman E, Carzaniga R, Evans ND, McComb DW, Porter AE, et al.: The role of intracellular calcium phosphate in osteoblast-mediated bone apatite formation. *Proc Natl Acad Sci U.S.A* 109(35): 14170-14175, 2012.

Campos JM, Sousa AC, Pinto PO, Ribeiro J, França ML, Caseiro AR, et al.: Application of Bonelike® as synthetic bone graft in orthopaedic and oral surgery in veterinary clinical cases. *Biomater Res* 22(1): 1-13, 2018.

Chen QZ, Thompson ID, Boccaccini AR: 45S5 Bioglass®-derived glass–ceramic scaffolds for bone tissue engineering. *Biomaterials* 27(11): 2414-2425, 2006.

Chen S, Jian Z, Huang L, Xu W, Liu S, Song D, et al.: Mesoporous bioactive glass surface modified poly (lactic-co-glycolic acid) electrospun fibrous scaffold for bone regeneration. *Int J Nanomedicine* 10: 3815-3827, 2015.

Daar AS, Greenwood HL: A proposed definition of regenerative medicine. *J Tissue Eng Regen Med* 1(3): 179-184, 2007.

Daculsi G: Biphasic calcium phosphate concept applied to artificial bone, implant coating and injectable bone substitute. *Biomaterials* 19(16): 1473-1478, 1998.

Danhier F, Ansorena E, Silva JM, Coco R, Le Breton A, Préat V: PLGA-based nanoparticles: an overview of biomedical applications. *J Control Release* 161(2): 505-522, 2012.

Dashnyam K, El-Fiqi A, Buitrago JO, Perez RA, Knowles JC, Kim H-W: A mini review focused on the proangiogenic role of silicate ions released from silicon-containing biomaterials. *J Tissue Eng* 8: 1-13, 2017.

de Alencar PGC, Vieira IFV: Bone banks. *Rev Bras Ortop (Sao Paulo) (English Edition)* 45(6): 524-528, 2010.

Demirkiran H, Hu Y, Zuin L, Appathurai N, Aswath PB: XANES analysis of calcium and sodium phosphates and silicates and hydroxyapatite–Bioglass® 45S5 co-sintered bioceramics. *Mater Sci Eng C* 31(2): 134-143, 2011.

Denhardt DT, Guo X: Osteopontin: a protein with diverse functions. *FASEB J* 7(15): 1475-1482, 1993.

Denry I, Kuhn LT: Design and characterization of calcium phosphate ceramic scaffolds for bone tissue engineering. *Dent Mater* 32(1): 43-53, 2016.

Dziemidowicz K, Sang Q, Wu J, Zhang Z, Zhou F, Lagaron JM, et al.: Electrospinning for healthcare: recent advancements. *J Mater Chem B* 9(4): 939-951, 2021.

Einhorn TA, Gerstenfeld LC: Fracture healing: mechanisms and interventions. *Nat Rev Rheumatol* 11(1): 45-54, 2015.

Erbetta CDAC, Alves RJ, Magalh J, de Souza Freitas RF, de Sousa RG: Synthesis and characterization of poly (D, L-lactide-co-glycolide) copolymer. J Biomater Nanobiotechnol 3(2): 208-225, 2012.

Fernández RF, Bucchi C, Navarro P, Beltrán V, Borie E: Bone grafts utilized in dentistry: an analysis of patients' preferences. *BMC Med Ethics* 16(1): 1-6, 2015.

Filipović B, Šošić-Jurjević B: *The Phytoestrogens, Calcitonin and Thyroid Hormones: Effects on Bone Tissue*, INTECH Open Acess Publisher, 2012.

Florencio-Silva R, Sasso GRdS, Sasso-Cerri E, Simões MJ, Cerri PS: Biology of bone tissue: structure, function, and factors that influence bone cells. *BioMed Res Int* 2015: 1-17, 2015.

Friederichs RJ, Brooks RA, Ueda M, Best SM: In vitro osteoclast formation and resorption of silicon-substituted hydroxyapatite ceramics. *J Biomed Mater Res A* 103(10): 3312-3322, 2015.

Gentile P, Chiono V, Carmagnola I, Hatton PV: An overview of poly (lactic-co-glycolic) acid (PLGA)-based biomaterials for bone tissue engineering. *Inter J Mol Sci* 15(3): 3640-3659, 2014.

Gentile P, Nandagiri VK, Daly J, Chiono V, Mattu C, Tonda-Turo C, et al.: Localised controlled release of simvastatin from porous chitosan–gelatin scaffolds engrafted with simvastatin loaded PLGA-microparticles for bone tissue engineering application. *Mater Sci Eng C* 59: 249-257, 2016.

Ghiasi MS, Chen J, Vaziri A, Rodriguez EK, Nazarian A: Bone fracture healing in mechanobiological modeling: A review of principles and methods. *Bone Rep* 6: 87-100, 2017.

Ghosal K, Chandra A, Praveen G, Snigdha S, Roy S, Agatemor C, et al.: Electrospinning over solvent casting: tuning of mechanical properties of membranes. *Sci Rep* 8(1): 1-9, 2018.

Gough JE, Jones JR, Hench LL: Nodule formation and mineralisation of human primary osteoblasts cultured on a porous bioactive glass scaffold. *Biomaterials* 25(11): 2039-2046, 2004.

Gupta A, Kumar V: New emerging trends in synthetic biodegradable polymers–Polylactide: A critique. *Eur Polym J* 43(10): 4053-4074, 2007.

Habibovic P, Kruyt MC, Juhl MV, Clyens S, Martinetti R, Dolcini L, et al.: Comparative in vivo study of six hydroxyapatite-based bone graft substitutes. *J Orthop Res* 26(10): 1363-1370, 2008.

Hadjidakis DJ, Androulakis II: Bone remodeling. *Ann N Y Acad Sci* 1092(1): 385-396, 2006.

Hench LL: Genetic design of bioactive glass. *J Eur Ceram Soc 2*9(7): 1257-1265, 2009.

Hench LL, West JK: *Biological applications of bioactive glasses*. Harwood Academic Publishers, 1996.

Hench LL: The story of Bioglass®. *J Mater Sci: Mater Med* 17(11): 967-978, 2006.

Hench LL: Bioceramics: from concept to clinic. *J Am Ceram Soc* 74(7): 1487-1510, 1991.

Henkel J, Woodruff MA, Epari DR, Steck R, Glatt V, Dickinson IC, et al.: Bone regeneration based on tissue engineering conceptions—a 21st century perspective. *Bone Res* 1(1): 216-248, 2013.

Higuchi J, Fortunato G, Woźniak B, Chodara A, Domaschke S, Męczyńska-Wielgosz S, et al.: Polymer membranes sonocoated and electrosprayed with nano-hydroxyapatite for periodontal tissues regeneration. *Nanomaterials* 9(11):1625, 2019.

Hing KA: Bioceramic bone graft substitutes: influence of porosity and chemistry. *Int J Appl Ceram Technol* 2(3): 184-199, 2005.

Hong M-H, Hong HJ, Pang H, Lee H-J, Yi S, Koh W-G: Controlled release of growth factors from multilayered fibrous scaffold for functional recoveries in crushed sciatic nerve. *ACS Biomater Sci Eng* 4(2): 576-586, 2018.

Hong M-H, Kim S-M, Om J-Y, Kwon N, Lee Y-K: Seeding cells on calcium phosphate scaffolds using hydrogel enhanced osteoblast proliferation and differentiation. *Ann Biomed Eng* 42(7): 1424-1435, 2014a.

Hong M-H, Kim YH, Ganbat D, Kim D-G, Bae C-S, Oh DS: Capillary action: enrichment of retention and habitation of cells via micro-channeled scaffolds for massive bone defect regeneration. *J Mater Sci: Mater Med* 25(8): 1991-2001, 2014b.

Hoppe A, Güldal NS, Boccaccini AR: A review of the biological response to ionic dissolution products from bioactive glasses and glass-ceramics. *Biomaterials* 32(11):2757-2774, 2011.

Huang W, Day DE, Kittiratanapiboon K, Rahaman MNJJoMSMiM: Kinetics and mechanisms of the conversion of silicate (45S5), borate, and borosilicate glasses to hydroxyapatite in dilute phosphate solutions. J Mater Sci: Mater Med 17(7): 583-596, 2006.

Huang W, Yang S, Shao J, Li Y-P: Signaling and transcriptional regulation in osteoblast commitment and differentiation. *Front Biosci* 12: 3068-3092, 2007.

Hunter GK, Hauschka PV, Poole RA, Rosenberg LC, Goldberg HA: Nucleation and inhibition of hydroxyapatite formation by mineralized tissue proteins. *Biochem J* 317(1): 59-64, 1996.

Itoh S, Nakamura S, Kobayashi T, Shinomiya K, Yamashita K: Effect of electrical polarization of hydroxyapatite ceramics on new bone formation. *Calcif Tissue Int* 78(3): 133-142, 2006.

Jiang S, Jin W, Wang Y-N, Pan H, Sun Z, Tang R: Effect of the aggregation state of amorphous calcium phosphate on hydroxyapatite nucleation kinetics. *RSC Adv* 7(41): 25497-25503, 2017.

Jones JR, Brauer DS, Hupa L, Greenspan DCJIJoAGS: Bioglass and bioactive glasses and their impact on healthcare. *Int J Appl Glass Sci* 7(4): 423-434, 2016.

Jones JRJAb: Review of bioactive glass: from Hench to hybrids. *Acta Biomater* 9(1): 4457-4486, 2013.

Jose MV, Thomas V, Johnson KT, Dean DR, Nyairo E: Aligned PLGA/HA nanofibrous nanocomposite scaffolds for bone tissue engineering. *Acta Biomater* 5(1): 305-315, 2009.

Khan SN, Cammisa Jr FP, Sandhu HS, Diwan AD, Girardi FP, Lane JM: The biology of bone grafting. *J Am Acad Orthop Surg* 13(1): 77-86, 2005.

Kim K, Luu YK, Chang C, Fang D, Hsiao BS, Chu B, et al.: Incorporation and controlled release of a hydrophilic antibiotic using poly (lactide-co-glycolide)-based electrospun nanofibrous scaffolds. *J Controlled Release* 98(1): 47-56, 2004.

Kini U, Nandeesh B: Physiology of bone formation, remodeling, and metabolism. In: *Radionuclide and hybrid bone imaging*. Springer. 29-57, 2012.

Komori T: Regulation of osteoblast differentiation by transcription factors. *J cell Biochem* 99(5): 1233-1239, 2006.

Koshino T, Murase T, Takagi T, Saito T: New bone formation around porous hydroxyapatite wedge implanted in opening wedge high tibial osteotomy in patients with osteoarthritis. *Biomaterials* 22(12): 1579-1582, 2001.

Kumar P, Vinitha B, Fathima G: Bone grafts in dentistry. *J Pharm Bioallied Sci* 5(Suppl 1): S125-S127, 2013.

Kusindarta DL, Wihadmadyatami H: The role of extracellular matrix in tissue regeneration. In: *Tissue regeneration*. INTECH Open Acess Publisher, 2018.

Lacroix D: Biomechanical aspects of bone repair. In: *Bone repair biomaterials*. Elsevier. 53-64, 2019.

Langer R, Vacanti JP: Tissue engineering. *Science* 260(5110): 920-926, 1993.

Lee YJ, Lee J-H, Cho H-J, Kim HK, Yoon TR, Shin H: Electrospun fibers immobilized with bone forming peptide-1 derived from BMP7 for guided bone regeneration. *Biomaterials* 34(21): 5059-5069, 2013.

Li D, Xia Y: Electrospinning of nanofibers: reinventing the wheel? *Adv Mater* 16(14): 1151-1170, 2004.

Li H, Zhou C-R, Zhu M-Y, Tian J-H, Rong J-H: Preparation and characterization of homogeneous hydroxyapatite/chitosan composite scaffolds via in-situ hydration. *J Biomater Nanobiotechnol* 1(1): 42-49, 2010.

Livingston T, Ducheyne P, Garino J: In vivo evaluation of a bioactive scaffold for bone tissue engineering. *J Biomed Mater Res* 62(1): 1-13, 2002.

Loh QL, Choong C: Three-dimensional scaffolds for tissue engineering applications: role of porosity and pore size. *Tissue Eng Part B Rev* 19(6): 485-502, 2013.

Lomas R, Chandrasekar A, Board TN: Bone allograft in the UK: perceptions and realities. *Hip Int* 23(5): 427-433, 2013.

Luo H, Zhang Y, Wang Z, Yang Z, Tu J, Liu Z, et al.: Constructing three-dimensional nanofibrous bioglass/gelatin nanocomposite scaffold for enhanced mechanical and biological performance. *Chem Eng J* 326: 210-221, 2017.

Magri AMP, Fernandes KR, Assis L, Kido HW, Avanzi IR, da Cruz Medeiros M, et al.: Incorporation of collagen and PLGA in bioactive glass: in vivo biological evaluation. *Int J Biol Macromol* 134:869-881, 2019.

Marelli B, Ghezzi CE, Mohn D, Stark WJ, Barralet JE, Boccaccini AR, et al.: Accelerated mineralization of dense collagen-nano bioactive glass hybrid gels increases scaffold stiffness and regulates osteoblastic function. *Biomaterials* 32(34): 8915-8926, 2011.

Mocanu A, Cadar O, Frangopol PT, Petean I, Tomoaia G, Paltinean G-A, et al.: Ion release from hydroxyapatite and substituted hydroxyapatites in different immersion liquids: in vitro experiments and theoretical modelling study. *R Soc Open Sci* 8(1): 1-25, 2021.

Moimas L, Biasotto M, Di Lenarda R, Olivo A, Schmid C: Rabbit pilot study on the resorbability of three-dimensional bioactive glass fibre scaffolds. *Acta Biomater* 2(2): 191-199, 2006.

Mondal S, Hoang G, Manivasagan P, Moorthy MS, Nguyen TP, Phan TTV, et al.: Nano-

hydroxyapatite bioactive glass composite scaffold with enhanced mechanical and biological performance for tissue engineering application. *Ceram Int* 44(13):15735-15746, 2018.

Monier-Faugere M-C, Langub MC, Malluche HH: Bone biopsies: a modern approach. In: *Metabolic Bone Disease and Clinically Related Disorders*. Elsevier. 237-280e, 1998.

Moore WR, Graves SE, Bain GI: Synthetic bone graft substitutes. *ANZ J Surg* 71(6): 354-361, 2001.

Moorthi A, Saravanan S, Srinivasan N, Partridge N, Zhu J, Qin L, et al.: Synthesis, characterization and biological action of nano-bioglass ceramic particles for bone formation. *J Biomater Tissue Eng* 2(3): 197-205, 2012.

Moorthi A, Vimalraj S, Avani C, He Z, Partridge NC, Selvamurugan N: Expression of microRNA-30c and its target genes in human osteoblastic cells by nano-bioglass ceramic-treatment. *Int J Biol Macromol* 56: 181-185, 2013.

Mroz TE, Joyce MJ, Steinmetz MP, Lieberman IH, Wang JC: Musculoskeletal allograft risks and recalls in the United States. *J Am Acad Orthop Surg* 16(10): 559-565, 2008.

Murugan R, Rao KP, Kumar TS: Heat-deproteinated xenogeneic bone from slaughterhouse waste: Physico-chemical properties. *Bull Mater Sci* 26(5): 523-528, 2003.

Nair AK, Gautieri A, Chang S-W, Buehler MJ: Molecular mechanics of mineralized collagen fibrils in bone. *Nat Commun* 4(1): 1-9, 2013.

Nair LS, Laurencin CT: Biodegradable polymers as biomaterials. *Prog Polym Sci* 32(8-9): 762-798, 2007.

Najeeb S, Zafar MS, Khurshid Z, Siddiqui F: Applications of polyetheretherketone (PEEK) in oral implantology and prosthodontics. *J Prosthodont Res* 60(1): 12-19, 2016.

Nandi S, Roy S, Mukherjee P, Kundu B, De D, Basu D: Orthopaedic applications of bone graft & graft substitutes: a review. *Indian J Med Res* 132(1): 15-30, 2010.

Ojansivu M, Wang X, Hyväri L, Kellomäki M, Hupa L, Vanhatupa S, et al.: Bioactive glass induced osteogenic differentiation of human adipose stem cells is dependent on cell attachment mechanism and mitogen-activated protein kinases. *Eur Cells Mater* 35: 54-72, 2018.

Özcan M, Hotza D, Fredel MC, Cruz A, Volpato CAM: Materials and Manufacturing Techniques for Polymeric and Ceramic Scaffolds Used in Implant Dentistry. *J Compos Sci* 5(3): 78-99, 2021.

Panseri S, Montesi M, Hautcoeur D, Dozio SM, Chamary S, De Barra E, et al.: Bone-like ceramic scaffolds designed with bioinspired porosity induce a different stem cell

response. *J Mater Sci: Mater Med* 32(1): 1-12, 2021.

Qi R, Guo R, Zheng F, Liu H, Yu J, Shi X: Controlled release and antibacterial activity of antibiotic-loaded electrospun halloysite/poly (lactic-co-glycolic acid) composite nanofibers. *Colloids Surf B* 110: 148-155, 2013.

Raggatt LJ, Partridge NC: Cellular and molecular mechanisms of bone remodeling. *J Biol Chem* 285(33): 25103-25108, 2010.

Rahaman MN, Day DE, Bal BS, Fu Q, Jung SB, Bonewald LF, et al.: Bioactive glass in tissue engineering. *Acta Biomater* 7(6): 2355-2373, 2011.

Rath SN, Nooeaid P, Arkudas A, Beier JP, Strobel LA, Brandl A, et al.: Adipose-and bone marrow-derived mesenchymal stem cells display different osteogenic differentiation patterns in 3D bioactive glass-based scaffolds. *J Tissue Eng Regen Med* 10(10): E497-E509, 2016.

Robb B, Lennox B: The electrospinning process, conditions and control. In: *Electrospinning for tissue regeneration*. Elsevier. 51-66, 2011.

Roberts TT, Rosenbaum AJ: Bone grafts, bone substitutes and orthobiologics: the bridge between basic science and clinical advancements in fracture healing. *Organogenesis* 8(4):114-124, 2012.

Samavedi S, Whittington AR, Goldstein AS: Calcium phosphate ceramics in bone tissue engineering: a review of properties and their influence on cell behavior. *Acta Biomater* 9(9): 8037-8045, 2013.

Santos Jr A, de Carvalho Zavaglia C: Tissue Engineering Concepts. In: *Reference Module in Materials Science and Materials Engineering*. Elsevier, 2016.

Sartori M, Giavaresi G, Parrilli A, Ferrari A, Aldini NN, Morra M, et al.: Collagen type I coating stimulates bone regeneration and osteointegration of titanium implants in the osteopenic rat. *Int Orthop* 39(10): 2041-2052, 2015.

Schmidt AH: Autologous bone graft: Is it still the gold standard? *Injury* 52(Suppl 2): S18-S22, 2021.

Shapiro F: Developmental bone biology. In: *Pediatric Orthopedic Deformities,* 1: 1-158, Springer. 2016.

Shie M-Y, Ding S-J, Chang H-C: The role of silicon in osteoblast-like cell proliferation and apoptosis. *Acta Biomater* 7(6): 2604-2614, 2011.

Si J, Wang C, Zhang D, Wang B, Hou W, Zhou Y: Osteopontin in bone metabolism and bone diseases. *Medical Sci Monit:* 26: e919159-e919151, 2020.

Stoddart MJ, Craft AM, Pattappa G, Gardner OF: *Developmental Biology and*

Musculoskeletal Tissue Engineering: Principles and Applications. Academic Press, 2018.

Sun B, Long Y, Zhang H, Li M, Duvail J, Jiang X, et al.: Advances in three-dimensional nanofibrous macrostructures via electrospinning. *Prog in Polym Sci* 39(5): 862-890, 2014.

Sun JY, Yang YS, Zhong J, Greenspan DC: The effect of the ionic products of Bioglass® dissolution on human osteoblasts growth cycle in vitro. *J Tissue Eng Regen Med* 1(4): 281-286, 2007.

Tamariz E, Rios-Ramírez A: Biodegradation of medical purpose polymeric materials and their impact on biocompatibility. In: *Biodegradation-Life of Science*: INTECH Open Acess Publisher, 2013.

Tavakol M, Vaughan TJ: The structural role of osteocalcin in bone biomechanics and its alteration in Type-2 Diabetes. *Sci Rep* 10(1): 1-10, 2020.

Tsigkou O, Jones JR, Polak JM, Stevens MM: Differentiation of fetal osteoblasts and formation of mineralized bone nodules by 45S5 Bioglass® conditioned medium in the absence of osteogenic supplements. *Biomaterials* 30(21): 3542-3550, 2009.

Varma S, Orgel JP, Schieber JD: Nanomechanics of type I collagen. *Biophys J* 111(1):50-56, 2016.

Vergnol G, Ginsac N, Rivory P, Meille S, Chenal JM, Balvay S, et al.: In vitro and in vivo evaluation of a polylactic acid-bioactive glass composite for bone fixation devices. *J Biomed Mater Res B* 104(1): 180-191, 2016.

Von Euw S, Wang Y, Laurent G, Drouet C, Babonneau F, Nassif N, et al.: Bone mineral: new insights into its chemical composition. *Sci Rep* 9(1): 1-11, 2019.

Vroman I, Tighzert L: Biodegradable polymers. *Materials* 2(2): 307-344, 2009.

Wang W, Yeung KW: Bone grafts and biomaterials substitutes for bone defect repair: A review. *Bioact Mater* 2(4): 224-247, 2017.

Wang X, Wu X, Xing H, Zhang G, Shi Q, E L, et al.: Porous nanohydroxyapatite/collagen scaffolds loading insulin PLGA particles for restoration of critical size bone defect. *ACS Appl Mater Interfaces* 9(13): 11380-11391, 2017.

Wang X, Zhang G, Qi F, Cheng Y, Lu X, Wang L, et al.: Enhanced bone regeneration using an insulin-loaded nano-hydroxyapatite/collagen/PLGA composite scaffold. *Int J Nanomedicine* 13: 117-127, 2018.

Wu ZY, Hill RG, Yue S, Nightingale D, Lee PD, Jones JR: Melt-derived bioactive glass scaffolds produced by a gel-cast foaming technique. *Acta Biomater* 7(4): 1807-1816, 2011.

Xiong J, O'Brien CA: Osteocyte RANKL: new insights into the control of bone remodeling. *J Bone Miner Res* 27(3): 499-505, 2012.

Xu F, Teitelbaum SL: Osteoclasts: new insights. *Bone Res* 1(1): 11-26, 2013.

Xu HH, Wang P, Wang L, Bao C, Chen Q, Weir MD, et al.: Calcium phosphate cements for bone engineering and their biological properties. *Bone Res* 5(1): 1-19, 2017.

Zhao D, Zhu T, Li J, Cui L, Zhang Z, Zhuang X, et al.: Poly (lactic-co-glycolic acid)-based composite bone-substitute materials. *Bioact Mater* 6(2): 346-360, 2021.

Zhao H, Wang G, Hu S, Cui J, Ren N, Liu D, et al.: In vitro biomimetic construction of hydroxyapatite–porcine acellular dermal matrix composite scaffold for MC3T3-E1 preosteoblast culture. *Tissue Eng Part A* 17(5-6): 765-776, 2011.

Zhou T, Liu X, Sui B, Liu C, Mo X, Sun J: Development of fish collagen/bioactive glass/chitosan composite nanofibers as a GTR/GBR membrane for inducing periodontal tissue regeneration. *Biomed Mater* 12(5): 055004, 2017.

Zimmermann G, Moghaddam A: Allograft bone matrix versus synthetic bone graft substitutes. *Injury* 42: S16-S21, 2011.

ABSTRACT (IN KOREAN)

45S5 생체활성 유리 및 폴리(락트산-코-글리콜산) 복합 마이크로섬유가 덮인 다공성 수산화인회석 지지체의 골 형성 효과

< 지도교수 권 재 성 >

연세대학교 대학원 응용생명과학과

류 정 현

구강, 두개악안면, 정형외과 등 의료 분야에서 다양한 합성골 이식재가 스캐폴드로 사용되고 있다. 이러한 재료 중 하나는 다공성 수산화인회석 (HAp) 지지체로 생체적합성과 골전도 특성을 가지고 있다. 그러나 생체활성과 골유도 특성 측면에서 한계가 있다. 한편, 45S5 생체활성유리(45S5 BG)는 생체활성, 골전도, 골유도 특성이 높은 것으로 잘 알려져 있다. 또한, 폴리(락트산-코-글리콜산)(PLGA)는 분해속도를 제어하는 특성으로 잘 알려진 생분해성 고분자이다. 이에 본 연구의 목적은 HAp 지지체의 단점을 보완하기 위해 PLGA/45S5 BG 복합 나노 섬유로 코팅된 HAp 지지체(HPB 지지체)를 제작하고 HPB 지지체의 특성을 심층적으로 분석하는 것이다.

연구를 수행하기 위하여 스폰지 복제법과 전기방사법으로 HPB 지지체를 제작하였다. 스피닝 시간은 실험군에 따라 10분, 20분, 그리고 30분으로 설정하였다. HPB 지지체는 주사전자현미경-에너지 X선 분광법, 마이크로 컴퓨터 단층 촬영, 열중량 분석을 사용하여 분석하였다. 또한, 유도쌍 플라스마 질량분석법으로 이온 방출을 28일 동안 관찰하였다. L929세포와 MC3T3-E1 세포를 배양하고 세포 독성, 세포 증식 및 세포 생존력을 평가하였다. 골형성 분화를 확인하기 위하여 ALP 활성도, western blot, 면역세포화학법, Alizarin Res S (ARS) 염색을 시행하였다. 각 검정의 결과는 일원분산 분석과 Tukey 사후 통계 검정으로 통계적 분석을 시행하였다 ($p < 0.05$).

모든 HPB 지지체는 주사전자현미경-에너지 X선 분광법을 통해 다공성 구조를 확인하였고 45S5 BG/PLGA 복합 마이크로 섬유 층으로 덮여 있다는 것을 확인하였다. 또한, HAp 구성원소 (Ca과 P)와 45S5 BG 구성 원소(Si, Ca, Na과 P)를 포함하고 있다는 것을 확인하였다. 마이크로 컴퓨터 단층 촬영법을 통해 HPB 지지체의 다공도는 89.2%로 해면골의 다공도와 유사하다는 것을 확인하였다. 모든 HPB 지지체의 45S5 BG/PLGA 마이크로 섬유는 열중량 분석에서 PLGA 마이크로섬유에 45S5 BG가 포함되었다는 것을 확인하였다. 또한, HPB 지지체는 28 일 동안 Si, Ca, Na, 그리고 P 이온이 지속적으로 방출한 것을 확인하였다. 모든 HPB 지지체의 세포 독성은 유의한 차이가 없었다. HPB 지지체의 세포 증식은 1일보다 3일에서 증가한 것을 확인하였다($p < 0.05$). ALP 활성도와 western blot 분석은 HPB20과 HPB30 지지체가 다른 지지체들에 비해 더 높게 골 형성이 되었다는 것을 확인하였다($p < 0.05$). 또한, 면역세포화학법을 통해 HPB 지지체에서 Osteopontin이 발현되었다는 것

을 확인하였다. 마지막으로, ARS 염색에서 30분 코팅된 HPB 지지체가 다른 지지체들보다 광물화 측면에서 더 효과적인 것을 확인하였다($p < 0.05$).

본 연구 결과, HPB 지지체는 스펀지 복제법과 전기방사법 두 가지 방법을 이용하여 성공적으로 제작하였다. 또한, 45S5 BG 구성 원소의 이온들이 서방형으로 방출된 것을 보여주었다. 또한, HPB 지지체는 골 유전자 발현으로 전조골세포의 증식 및 조골세포의 분화에 모두 효과적이었다. 따라서 HPB 지지체는 골 형성 활성을 위하여 잠재적인 골 대체물이 될 수 있음을 시사하였다.

핵심 되는 말: 수산화인회석, 45S5 생체활성유리, 폴리(락트산-코-글리콜산), 골 형성 활성도, 생체 활성도